

NPS67-81-017

AD A 115263

NAVAL POSTGRADUATE SCHOOL

Monterey, California



THESIS

FLOW CONTROL FOR A HIGH
ENERGY LASER TURRET USING
TRAPPED VORTICES STABILIZED BY SUCTION

by

James Edward Burd

December 1981

Thesis Advisor:

A. E. Fuhs

Approved for public release; distribution unlimited

Prepared for: Captain Richard deJonckheere
Air Force Weapons Laboratory
Kirtland Air Force Base
New Mexico 87117

DTIC FILE COPY

ited DTIC
S ELECTE
JUN 07 198

82 43 00 836

NAVAL POSTGRADUATE SCHOOL
Monterey, California

Rear Admiral J. J. Ekelund
Superintendent

David A. Schrady
Acting Provost

This thesis prepared in conjunction with research supported
in part by the Air Force Weapons Laboratory, Kirtland Air
Force Base, New Mexico 87117.

Reproduction of all or part of this report is authorized.

Released as a
Technical Report by:


W. M. TOLLES

Dean of Research

UNCLASSIFIED

SECURITY CLASSIFICATION OF THIS PAGE (When Data Entered)

UNCLASSIFIED

SECURITY CLASSIFICATION OF THIS PAGE/When Data Entered.

>One technique proposed for flow control is a fairing design which will stabilize shed vortices by suction. A two dimensional computer model was used to design a fairing compatible with present test equipment.

Experimental research of this fairing design was conducted in wind tunnel tests. Although flow mapping demonstrated improved flow performance through the use of suction, total quiescent flow was never achieved. A more adequate three dimensional model is needed to design a fairing that will stabilize trapped vortices.,

Accession For	
NTIS GRA&I	<input checked="" type="checkbox"/>
DTIC TAB	<input type="checkbox"/>
Unannounced	<input type="checkbox"/>
Justification	
By _____	
Distribution/ _____	
Availability Codes	
Dist	Avail and/or Special
A	



Approved for public release; distribution unlimited

Flow Control for a High Energy Laser Turret
Using Trapped Vortices Stabilized by Suction

by

James Edward Burd
Lieutenant, United States Navy
B.S., United States Naval Academy, 1975

Submitted in partial fulfillment of the
requirements for the degree of

MASTER OF SCIENCE IN AERONAUTICAL ENGINEERING

from the

NAVAL POSTGRADUATE SCHOOL
December 1981

Author:

James E. Burd

Approved by:

Allen E. Fuchs
Thesis Advisor

Mos F. Schwartz
Chairman, Department of Aeronautics

William M. Teller
Dean of Science and Engineering

ABSTRACT

The Department of Defense is concerned with the viability of an airborne high energy laser system. The laser is housed in a blunt turret atop a NKC-135 aircraft. Turbulence generated by flow separation around the turret causes optical distortion of the laser beam. Control of flow separation is needed to improve laser beam performance especially for aft-aimed turrets.

One technique proposed for flow control is a fairing design which will stabilize shed vortices by suction. A two dimensional computer model was used to design a fairing compatible with present test equipment.

Experimental research of this fairing design was conducted in wind tunnel tests. Although flow mapping demonstrated improved flow performance through the use of suction, total quiescent flow was never achieved. A more adequate three dimensional model is needed to design a fairing that will stabilize trapped vortices.

COMMENT CONCERNING JOINT RESEARCH EFFORT

This thesis and LCDR David Rippel's thesis, Airborne Laser Turret Flow Control: A Parametric Study of Wind Tunnel Conditions [Ref. 1], were the result of a joint research effort. The basic data acquisition system was the same for both projects, however this thesis deals with the quality of flow using a nosepiece designed to stabilize shed vortices. The results in Ref. 1 are a more complete testing of two earlier nosepiece designs.

TABLE OF CONTENTS

I.	INTRODUCTION	14
A.	BACKGROUND	14
B.	THESIS OBJECTIVE	15
II.	VORTEX THEORY	16
A.	VORTEX GENERATION	16
1.	Boundary Layer Separation	16
2.	Von Kármán Vortex Street	18
B.	VORTEX MOTION	19
1.	Forced Vortex Motion	19
2.	Free Vortex Motion	19
3.	Rankine Combined Vortex	19
C.	IMPROVED VORTEX VELOCITY DISTRIBUTION	20
1.	Core Flow	20
2.	Burgers-Rott Solution	20
III.	NOSEPIECE DESIGN	22
A.	DESIGN PARAMETERS	22
B.	ELECTROSTATIC DESIGN	23
C.	COMPUTER DESIGN	24
1.	Panel Method	24
2.	Input Parameters	26
3.	Output Parameters	27
IV.	EXPERIMENTAL APPARATUS	30

A.	WIND TUNNEL	30
B.	BLOWER	30
C.	DUCTING	31
D.	FAIRING	31
E.	TURRET	32
F.	NOSEPIECE	32
G.	INSTALLATION	32
V.	INSTRUMENTATION	34
A.	PRESSURE TAPS	34
B.	DATA ACQUISITION SYSTEM	34
C.	TUFTS	35
VI.	EXPERIMENTAL RESULTS	36
A.	TEST PROCEDURE	36
1.	No Suction	36
2.	Suction Through a 2.5 Inch Diameter Hole .	36
3.	Suction with the Aft Area Covered	36
4.	Suction with the Forward Area Covered . . .	37
5.	Suction Through a 2 Inch Slot	37
6.	Suction Through the Porous Plate	37
7.	Suction Through Large Uncovered Holes . . .	37
B.	FLOW MAPPING RESULTS	38
1.	No Suction	38
2.	Suction Through a 2.5 Inch Diameter Hole .	38
3.	Suction with the Aft Area Covered	39
4.	Suction with the Forward Area Covered . . .	39

5. Suction Through a 2 Inch Slot	39
6. Suction Through the Porous Plate	40
7. Suction Through Large Uncovered Holes . .	40
C. PRESSURE COEFFICIENT RESULTS	40
VII. CONCLUSIONS AND RECOMMENDATIONS	42
A. CONCLUSIONS	42
B. RECOMMENDATIONS	42
APPENDIX A. EVALUATION OF THE PRESSURE COEFFICIENT . .	43
TABLES	44
FIGURES	54
COMPUTER PROGRAM	92
LIST OF REFERENCES	95
INITIAL DISTRIBUTION LIST	98

LIST OF TABLES .

III-1.	COORDINATES OF INITIAL PANEL DESIGN	44
III-2.	COORDINATES OF NOSEPIECE VARIATIONS	46
III-3.	COORDINATES OF FINAL PANEL DESIGN	49
III-4.	TANGENTIAL VELOCITIES AND PRESSURE COEFFICIENTS OF FINAL PANEL DESIGN	51
VI-1.	PRESSURE COEFFICIENTS OF NOSEPIECE	53

LIST OF FIGURES

I-1.	TRAPPED VORTEX/SUCTION FAIRING FROM CRAIG [Ref. 3]	54
II-1.	FROM PAO [Ref. 5], STREAMLINE FLOW AND PRESSURE DISTRIBUTIONS FOR A CYLINDER	55
II-2.	VELOCITY DISTRIBUTION OF A FORCED VORTEX . . .	56
II-3.	VELOCITY DISTRIBUTION OF A FREE VORTEX	56
II-4.	VELOCITY DISTRIBUTION OF A RANKINE COMBINED VORTEX	56
II-5.	NORMALIZED GRAPH OF THE BURGERS-ROTT AND RANKINE VELOCITY DISTRIBUTIONS	57
III-1.	FIXED AND VARIABLE GEOMETRIC PARAMETERS OF COMPONENTS (TOP VIEW LOOKING DOWN)	58
III-2.	SIDE VIEW OF COMPONENTS WITH FIXED AND VARIABLE GEOMETRIC PARAMETERS	59
III-3.	TEST SETUP FOR EQUIPOTENTIAL PLOTTING	60
III-4.	DESIGN PHILOSOPHY FOR MATCHED VORTEX AND STREAMLINE FLOW	61
III-5.	INITIAL PANEL DESIGN	62
III-6.	FIRST NOSEPIECE DESIGN VARIATION	63
III-7.	SECOND NOSEPIECE DESIGN VARIATION	64
III-8.	THIRD NOSEPIECE DESIGN VARIATION	65
III-9.	TANGENTIAL VELOCITY PLOT	66
III-10.	COMPLETED DESIGN, SIDE VIEW	67
III-11.	COMPLETED DESIGN, TOP VIEW	68
III-12.	COMPLETED DESIGN, END VIEW	69
IV-1.	BLOWER AND DUCTWORK UNDERNEATH TUNNEL	70

IV-2.	PLENUM CHAMBER AND FAIRING (NOSEPIECE AND TURRET REMOVED)	71
IV-3.	BLOWER AND DUCTWORK, BACK SIDE	72
IV-4.	FILLER PIECE CONSTRUCTION	73
IV-5.	NOSEPIECE, TOP VIEW	74
IV-6.	NOSEPIECE, SIDE VIEW	75
IV-7.	COMPLETE MODEL ASSEMBLY	76
IV-8.	COMPLETE MODEL ASSEMBLY	77
IV-9.	SIDE VIEW OF WIND TUNNEL MODEL AND BLOWER INSTALLATION	78
IV-10.	BASE PLATFORM WITH ADJUSTABLE HOLE CONTROLS . .	79
V-1.	TURRET PRESSURE TAP LOCATIONS	80
V-2.	NOSEPIECE PRESSURE TAP LOCATIONS	81
V-3.	DATA ACQUISITION SYSTEM	82
V-4.	SCANIVALVE	83
VI-1.	FLOW MAPPING, NO SUCTION	84
VI-2.	FLOW MAPPING, SUCTION THROUGH A 2.5 INCH DIAMETER HOLE	85
VI-3.	FLOW MAPPING, SUCTION WITH AFT AREA CLOSED . .	86
VI-4.	FLOW MAPPING, SUCTION WITH FORWARD AREA CLOSED	87
VI-5.	FLOW MAPPING, SUCTION THROUGH 2 INCH SLOT . . .	88
VI-6.	FLOW MAPPING, SUCTION THROUGH POROUS PLATE . .	89
VI-7.	FLOW MAPPING, SUCTION WITH LARGE HOLE OPEN . .	90
VI-8.	EXPERIMENTAL DATA PLOTTED WITH THEORETICAL PRESSURE DISTRIBUTION OF A CYLINDER	91

ACKNOWLEDGMENTS

I would like to acknowledge the support of Captain Richard deJonckheere, USAF, and the Air Force Weapons Laboratory for providing the funding necessary to conduct this research effort. I would also like to thank Lieutenant Commander David Rippel for his gracious assistance throughout the course of our project.

Most of all, I am very grateful to Dr. Allen E. Fuhs, Distinguished Professor of Aeronautics, for his support, guidance, and technical expertise. As a thesis advisor, Dr. Fuhs spent many hours of his busy schedule with me in order to ensure the successful completion of this research problem. I am also grateful to Dr. Peter Bellamy-Knights and Dr. Oded Amichai for their extra time spent on the program for computer design.

I would like to thank Supervisory Aerospace Engineering Technicians Robert Besel and Ted Dunton and Electronics Technician Ray Garcia for their technical aid throughout my tour at the Naval Postgraduate School. I would also like to commend Model Shop Technician Ronald Ramaker for his superb effort in building a very complex, three dimensional design. Without his amazing talents, this project could not have been finished.

Finally, I would like to thank my dear wife, Nancy, for her expert typing, eager help, and "gentle" yet constant persuasion. Without her undying support, I would have never gotten this far.

I. INTRODUCTION

A. BACKGROUND

Over the years the Department of Defense (DOD) has been concerned with the deployment of a high energy laser as a viable weapons system. Airborne laser research is being conducted at the Air Force Weapons Laboratory, Kirtland Air Force Base, New Mexico. Two technically complex NKC-135 aircraft are being used as the airborne laboratories.

The high energy laser weapon system radiates large amounts of thermal energy on another airborne target rendering it useless. The main components of the system include the laser itself and the beam control subsystem. The turret on top of the NKC-135 aircraft houses the pointer-tracker assembly which aims the laser beam. Due to the blunt body design inherent with the rounded laser turret, shear layers, boundary layers, flow separation, and vortex shedding can cause noticeable distortions in the laser beam energy. Unsteady pressure loads on the turret and optical components cause jitter, a phenomenon that translates beam energy focused on a small area into a larger area. The time needed to inflict damage to the target is increased.

Separated flow must be controlled in order to enhance optical qualities of the laser beam. Research and experimentation have demonstrated that optical distortion caused

by unsteady flow cannot be corrected by adaptive optical systems due to the bandwidth requirements exceeding current technology.

Various methods for attempting flow control over a turret were introduced at a workshop sponsored by Captain Richard deJonckheere at the Air Force Weapons Laboratory, Kirtland Air Force Base, New Mexico [Ref. 2]. One innovative method discussed in this workshop was an attempt to trap vortices shed by the turret and stabilize them by suction through ports located in the most optimum locations. This stabilization could then hopefully create quiescent flow patterns over the surface of the turret. Figure I-1 is the original design submitted by Craig [Ref. 3].

B. THESIS OBJECTIVE

The primary objective of this thesis research was to design, manufacture, and test a fairing-nosepiece device which would employ suction to stabilize trapped vortices shed by a laser turret. A design compatible with previous test equipment was necessary. The suction holes would be in the wind tunnel floor.

II. VORTEX THEORY

A. VORTEX GENERATION

1. Boundary Layer Separation

Viscosity is that property of a real fluid which creates shear forces between two fluid elements. Air and water both have small viscosities; therefore in earlier days, scientists assumed that forces due to viscous friction were negligible compared with pressure and gravity forces. The science of classical hydrodynamics is based on the premise that fluid is ideal, i.e., frictionless and incompressible. Empirical results, however, did not always agree with classical fluid theories. This is especially true when a solid body is immersed in a fluid flow. Classical hydrodynamic calculations lead to zero drag on the immersed body, which is impossible. This contradiction is referred to as d'Alembert's paradox, and it was two centuries before a solution to the problem was discovered. The concept of the boundary layer, theorized by L. Prandtl in 1904 [Ref. 4], bridged this scientific gap. He deduced that the fluid flow is divided into two regions. The fluid near the solid surface is in a thin boundary layer where the velocity gradient is large enough that friction within the boundary layer due to fluid viscosity must be considered. The other region is outside the boundary layer and the effect of fluid viscosity

is negligible. Fluid in the outer region follows classical potential flow theories.

Pressure is a force exerted on a unit area and a pressure gradient is a change in pressure along a particular direction. When there is an adverse pressure gradient (pressure increasing in the downstream direction) the boundary layer thickens rapidly along the surface. Adverse pressure gradients act to oppose the downstream fluid motion and reduce the fluid momentum in the boundary layer area. High viscous frictional forces in the area next to the surface tend to retard the flow velocity even more. The combination of the opposing pressure and the viscous frictional forces can ultimately cause the phenomenon of flow separation. When the flow separates, large turbulent eddies can be formed.

The position of the point of separation is dependent on the roughness of the body, the Reynolds number of the flow, and the geometric curvature of the body. By examining an irrotational form of Bernoulli's equation

$$\frac{p_1}{\rho_1} + \frac{v_1^2}{2} = \frac{p_2}{\rho_2} + \frac{v_2^2}{2} \quad (2-1)$$

it can be seen that adverse pressure gradients are generally created when there is a deceleration of the fluid motion.

For example, if V_2 is smaller than V_1 , then p_2 is larger than p_1 , providing the density does not change.

Flow mapping over a cylinder can be seen in Figure II-1, taken from Pao [Ref. 5]. Part (a) shows the streamline pattern and pressure distribution for a non-viscous flow. Part (b) shows a laminar boundary layer separation due to the decelerated flow in the rear portion of the cylinder. Part (c) also shows a separated flow, but the separation points are farther downstream caused by an increase in fluid momentum generated by a turbulent flow.

2. Von Kármán Vortex Street

Von Kármán noted that when a cylindrical body is moved through a fluid, a series of alternating vortices are generated. Generally the vortices along one line all have circulation in the same direction, but are opposite to the vortices in the other line [Ref. 6]. A. Roshko at California Institute of Technology, Pasadena, also studied the vortex street phenomenon and determined that the formation and shape of the vortices are highly dependent on the Reynolds number [Ref. 7, 8]. At higher Reynolds numbers, turbulence breaks down vortex street periodicity. During this process the distance between individual vortices increases steadily while the circulation decreases [Ref. 8: p. 222].

B. VORTEX MOTION

1. Forced Vortex Motion

A forced vortex motion occurs when a constant torque is maintained on a body of fluid. This is illustrated when a circular container of fluid is rotated about its central axis with a constant angular momentum [Ref. 5: pp. 139-140]. The velocity of any fluid particle is proportional to the radius outward from the axis of rotation

$$v = rC_1 \quad (2-2)$$

Figure II-2 shows the velocity distribution of a forced vortex motion.

2. Free Vortex Motion

A free vortex motion occurs naturally when fluid masses move in curved paths. The velocity of a free vortex motion is seen to vary inversely with the radial distance from the vortex center

$$v = \frac{C_2}{r} \quad (2-3)$$

Figure II-3 depicts the free vortex velocity distribution.

3. Rankine Combined Vortex

The velocity of flow in a free vortex would go to infinity as the radius goes to zero. This, however, is physically impossible due to viscous forces at the central region. The resulting flow resembles the simple case Rankine

combined vortex, which is a combination of forced and free vortex motion. Circular air flow in a tornado is an approximation of a Rankine combined vortex. Figure II-4 is an illustration of the Rankine combined vortex velocity distribution.

C. IMPROVED VORTEX VELOCITY DISTRIBUTION

1. Core Flow

Various efforts have been described in Lewellen [Ref. 9] to improve upon the velocity distribution in order to smooth the sharp discontinuity between the combined forced and free vortex motions. The Rankine vortex is the simplest solution to the angular momentum equation noted in Ref. 9. The angular momentum equation is

$$\frac{D(vr)}{Dt} = vr \left\{ \frac{\partial}{\partial r} \left(\frac{1}{r} \frac{\partial (vr)}{\partial r} \right) + \frac{\partial^2 v}{\partial z^2} \right\} \quad (2-4)$$

This equation does assume that the core of the tornado is axisymmetric and that the eddy viscosity, ν , is constant.

2. Burgers-Rott Solution

Lewellen [Ref. 9] notes that a well-behaved solution to equation (2-4) was obtained by Burgers and Rott independently. For their solution, consider a cylindrical coordinate system with velocity components u , v , and w . The radial inflow velocity, u , is defined as

$$u = -ar \quad (2-5)$$

The axial flow velocity, w , is

$$w = 2az \quad (2-6)$$

while the tangential velocity, v , is defined as

$$v = \frac{\Gamma_\infty}{r} \left[1 - \exp\left(\frac{-ar^2}{2v}\right) \right] \quad (2-7)$$

The variable, a , used in all three velocity components, is the upflow gradient and has the units of 1/sec. The pressure distribution consistent with this solution is

$$\begin{aligned} p(r,z) &= p(0,0) + \rho \frac{\Gamma_\infty^2 a}{v} \int_0^{\frac{ar^2}{2v}} \left(\frac{1-e^{-x}}{x} \right)^2 dx \\ &\sim \frac{\rho a^2}{2} (r^2 + 4z^2) - \rho gz \end{aligned} \quad (2-8)$$

The kinematic viscosity, ν , in equation (2-7) becomes the effective turbulent kinematic viscosity when the flow in the vortex is turbulent. A characteristic velocity for the flow is $\sqrt{a/\nu}$ and a characteristic length is $\sqrt{\nu/a}$. The velocity and radial distance in Figure II-5 have been normalized with respect to these characteristic quantities.

III. NOSEPIECE DESIGN

A. DESIGN PARAMETERS

Refer to Figures III-1 and III-2, where the four components are identified. These components include: turret, nosepiece, fairing, and plenum for suction at wind tunnel floor.

After the initial decision was made to study the possibilities of the trapped vortex nosepiece, a design process was begun. The new nosepiece was to be completely compatible with turret, fairing, and blower dimensions in order to prevent major modifications to the existing system. Results of the trapped vortex research could also be compared more easily with data obtained during experimentation of the Tapered Symmetric Nosepiece (TSN) and the Uniform Conformal Nosepiece (UCN) [Ref. 1, 11, and 12].

Fixed apparatus measurements included a fairing width of 10.5 inches, a turret diameter of 16.8 inches, and a plenum area 18 by 20 inches. A research effort was dedicated to determine critical values for the geometry. Figure III-1 is a top view, looking down on the wind tunnel floor. The solid lines represent fixed apparatus measurements, while the dashed lines represent variable geometric parameters. The length, L, is the distance between the center of the turret and the fairing. The fairing was fixed to the tunnel floor

and could not be moved. Nosepiece dimensions are determined by the length, L_2 , and the width, W . Suction port locations are determined by R_2 and W_2 . The variable, D , is the suction port diameter, while R is the radius that would define the curvature of the nosepiece. The turret-nosepiece-fairing assembly can also be seen in Figure III-2. Note that the values L_3 and L_4 determine the nosepiece length. Top nosepiece curvature is represented by the value R_3 , which is at a height, H , above the tunnel floor. Suction port area, vortex location, and nosepiece curvature were three of the more important design considerations.

B. ELECTROSTATIC DESIGN

During the early design stages, a method was needed to visualize flow patterns as influenced by different geometric design parameters. Electrostatic plotting seemed like an effective tool to use for problem modeling. The PASCO Model 224 Electrometer manufactured by PASCO Scientific, San Leandro, California, was used as a flow plotting device. Various nosepiece and fairing designs were tested in order to determine the effectiveness of this system. Figure III-3 shows the arrangement of the test design between the two electrodes. The electrodes and the test design were drawn with a silver conducting pen. Two leads were joined to points A and B in Figure III-3 and were connected to a variable potentiometer. Increasing current flow in these leads would be

akin to increased suction through base platform vortex ports. Lines of equipotential correspond to streamlines. The lines of equipotential which were then plotted around the entire test design represent the streamlines around an aerodynamic surface. However, the test apparatus was not precise enough in the area of the nosepiece to make design decisions. Further research attempts using the electrostatic analogy were cancelled.

C. COMPUTER DESIGN

Lack of success in the electrostatic design phase and the complexity of three dimensional mathematical models forced the use of a computer program geared to two dimensional flow.

1. Panel Method

A Fortran program, which was developed by Adjunct Professor Peter Bellamy-Knights, applied the panel method to determine velocity distributions and pressure coefficients over any aerodynamic surface. The surface could be divided into panels, each with its own source strength. An iterative routine using linear equations in matrix format solved for the magnitude of the source strengths, the velocities tangential to the panels, and the corresponding pressure coefficients.

In order to use the panel method for design, various additions were incorporated. The turret-nosepiece-fairing

assembly was assumed to be a one-piece body, symmetrical with respect to the X-axis. Two vortices of variable position and strength were located outside the nosepiece area; vortex location is shown in the top half of Figure III-4. The effects of these two vortices influenced the magnitude of all the other panel strengths, which in turn determined the final output. Design variations were necessary in the region of the nosepiece, therefore different coordinates could be input to describe the different panels. By varying nosepiece geometry, it was possible to deduce flow trends along the surface of the panels.

The two-dimensional flow conditions calculated using the panel method are not a precise representation of the actual flow for two reasons. First, the actual geometry is three-dimensional, and second, the calculation ignores viscous effects. Recognizing these deficiencies, a design philosophy was used. The design philosophy is illustrated in Figure III-4. Refer to the plane of symmetry in Figure III-4. Below the plane of symmetry is an equivalent solid body which results from a trapped vortex. Above the plane of symmetry is the flow with the trapped vortex. The line segment A-B in Figure III-4 is the dividing streamline between the external flow and the trapped vortex. Along streamline A-B is a distribution of pressure and velocity. The aim of the computer model was to match flow conditions, i.e. velocity and pressure, along streamline A-B. The flow

conditions along A-B due to the trapped vortex should be identical to flow conditions along A'-B' due to an equivalent solid body. A copy of the Fortran computer program is included at the end of this report.

2. Input Parameters

In order to allow easy transfer of coordinate inputs, all values were non-dimensionalized with respect to the turret radius. The turret-nosepiece-fairing assembly was divided into thirty total panels. More panels were positioned in areas of rapid slope changes such as the nosepiece and turret curves. Figure III-5 shows the basic breakdown of the initial panel design. Table III-1 gives the x and y coordinate values of all thirty points. Points 6 through 12 and their negative counterparts, 20 through 26, are completely variable and determine a design geometry of the nosepiece. Figures III-6, III-7 and III-8 illustrate other nosepiece variations which were calculated. Table III-2 gives the coordinate locations of these three other designs.

A model was needed to describe vortex strength. Consider fluid flow along a line in a volume. The dot product of the instantaneous velocity vector and a line element will produce the component of the velocity along that line. Circulation is the line integral of that dot product along a closed path. The mathematical expression for circulation is

$$\Gamma = \oint \vec{U} \cdot d\vec{s} \quad (3-1)$$

where U is the instantaneous velocity and ds is the line element. This equation can be non-dimensionalized by dividing both sides by the freestream velocity, U_∞ , and a characteristic length. The characteristic length in this case is the turret radius, R . The non-dimensional equation becomes

$$\frac{\Gamma}{U_\infty R} = \oint \left(\frac{\vec{U}}{U_\infty} \right) \cdot d\left(\frac{\vec{s}}{R} \right) \quad (3-2)$$

For a free vortex, the circulation is proportional to the strength of the free vortex. The computer program uses a variable F , which is equal to the value $\Gamma/U_\infty R$ from equation (3-2). Thus, F is used to describe non-dimensional vortex strength. As noted earlier, the two vortex locations and strengths were completely variable. The computer program inputs vortex data as X_2 , Y_2 , and F as the X-coordinate, Y-coordinate, and non-dimensional vortex strength respectively. The negative counterpart is automatically calculated in the computer program. The value of (F) was assumed to be 0.6 and kept as a constant parameter.

3. Output Parameters

The most important output parameter from the program was the tangential velocity vectors produced along the wall of the nosepiece panels. Plots were made of these vectors to determine the direction and strength of the flow field. The freestream velocity was taken as unity, thus a velocity

downstream could be compared to it. For example, if a velocity vector read a value of -0.5, the tangential velocity of that panel at its midpoint would be one-half the freestream value and in the opposite direction.

Figure III-7 demonstrated better flow conditions during calculations, but the design needed to be shortened to produce a stronger region of reversed flow along the panels.

Figure III-9 shows a plot of the final configuration and the tangential velocity vectors determined from the computer output. This configuration, coupled with the vortex location specified, proved to be the only design with a velocity magnitude of zero along the panel between points eleven and twelve. All other designs tested had a larger flow vector in the direction towards point twelve. Note how the velocity vectors changed direction at point A in Figure III-9. It was assumed that the flow would be forced to travel along a path, similar to the line A-B. This flow pattern is typical of the design philosophy noted before in Figure III-4.

The coordinates of the selected design were faired in, and a three dimensional body was constructed. The forward portion of the nosepiece was cut to meet the aft portion of the turret. Figures III-10, III-11, and III-12 show the final completed side, top, and end views respectively. Table III-3 gives the coordinates of the 30 points used in

the final panel design, while Table III-4 gives the tangential velocities and pressure coefficients along the panels of the design shown in Figure III-9.

IV. EXPERIMENTAL APPARATUS

A. WIND TUNNEL

Wind tunnel tests were conducted in the Naval Postgraduate School five-foot by five-foot low-speed tunnel at a maximum velocity of 33 feet per second. Using the previously built one-third scale turret model ($D = 16.8$ inches) a Reynolds number of about 3×10^5 was achieved. According to Schlichting [Ref. 10: pp. 20-21], the value of the Reynolds number for the tests was in the critical range and flow should be turbulent in the boundary layer on the turret.

B. BLOWER

The blower was chosen during previous thesis research [Ref. 11 and 12], and is the Backward Inclined Airfoil, Model 500, Single Width Single Inlet (B.I.A.-500, SWSI) made by the Aerovent Company Inc., of Piqua, Ohio. This centrifugal blower has a capacity of 7700 cfm with a static pressure differential of 14 inches H_2O . A control valve on the blower face could be operated from a full closed to full open position, allowing for an increase in airflow. A sheet metal structure was used to mate the blower inlet to the wooden ductwork underneath the tunnel test section. Figure IV-1 shows the front side of the blower and completed ductwork below the wind tunnel.

C. DUCTING

A wooden rectangular duct connected the hollow fairing to the blower assembly. Four adjustable butterfly valves were positioned inside four separate flow channels within the ductwork. A fifth channel led to a large plenum chamber at the base of the turret which was used in previous research as a path for fuselage boundary layer bleed. Figure IV-2 shows the fairing positioned behind the plenum chamber with the nosepiece and turret removed. The plenum duct also had a fifth butterfly valve which was locked in the full open position. Figure IV-3 shows the back side of the ductwork under the tunnel flooring and the five adjustable butterfly valves.

D. FAIRING

A filler piece six inches long was used to fill the gap between the previous fairing position and plenum cavity on the tunnel floor. The plenum chamber could now be used as a vortex suction unit without major modification of existing ductwork. Figure IV-4 shows the filler piece construction. The hollow fairing was not used as a suction device, so the four other butterfly valves were locked in the fully-closed position. The fairing was 10.5 inches wide, which produced a maximum look-back angle of 150 degrees.

E. TURRET

A hollow, one-third scale model of the existing airborne laser turret was constructed on drawings provided by Captain Richard deJonckheere. The wooden model consists of a hollow 16.8 inch diameter circular cylinder, 9.6 inches in height, topped by a 16.8 inch diameter hemisphere. Twenty-five individual pressure taps were placed over the area of the turret.

F. NOSEPIECE

The nosepiece was constructed from sheet metal, wood, and styrofoam. It was placed in between the fairing filler section and the laser turret. The upper one-third of the model was a three dimensional body based on the design criteria from Chapter III. Another nine pressure taps were located on the left side of the model. Figures IV-5 and IV-6 show the general shape of the nosepiece.

G. INSTALLATION

The plenum chamber was covered by a 27 x 27 inch square sheet of one-half inch plywood in order to create a base platform for the nosepiece and turret. Figures IV-7 and IV-8 show various views of the fairing, filler piece, turret and nosepiece. Figure IV-9 shows a side view drawing of the entire test setup. Various size holes were drilled in the base platform in order to suck the trapped vortices using

the blower assembly. Figure IV-10 shows the final configuration of the base platform and the adjustable hole control.

V. INSTRUMENTATION

A. PRESSURE TAPS

Pressure taps were installed in the turret, wind tunnel, and nosepiece. Due to the varied location of all the pressure taps, a pressure distribution of the turret and nosepiece surfaces could be plotted. Figure V-1 is a pictorial representation of the various pressure tap locations on the turret surface, while Figure V-2 shows the pressure tap locations on the left side of the nosepiece. All pertinent pressure taps were connected directly to a 48 port Scanivalve via flexible Tygon tubing.

B. DATA ACQUISITION SYSTEM

The wind tunnel data acquisition system used during the course of research included an INTEL 80/10 Computer System, an AN/UGC-59A Teletypewriter Set, a 48 port Scanivalve, and an analog to digital display box. Figure V-3 shows the computer system, teletypewriter, and digital display unit. Figure V-4 is a picture of the Scanivalve.

A master control program for Scanivalve operation was developed to ensure that voltage readings taken from the system could be displayed on the teletypewriter. These voltage readings from a capacitor pressure transducer in the Scanivalve were converted to pressure in centimeters of

water using a U-tube manometer. Due to the linearity of the various voltages plotted against different pressure values of the U-tube, an equation was determined to facilitate conversion

$$y = 9.2608x + 0.0269$$

where x is the value read from the teletypewriter and y is the pressure in centimeters of water. Knowing the pressure readings, velocities and pressure coefficients could then be calculated. Appendix A is an outline of the procedure used to find the pressure coefficients.

C. TUFTS

To visualize various flow patterns, tufts of yarn were taped over the turret, nosepiece, and base platform. Turbulent boundary layer flow in the turbulent separated region could be physically seen by the violent motions of individual tufts. Likewise, quiescent flows were demonstrated by non-moving tufts. A comprehensive flow mapping for various flow conditions is presented in the next chapter.

VI. EXPERIMENTAL RESULTS

A. TEST PROCEDURE

1. No Suction

The turret, nosepiece, base platform, and fairing were set up on the tunnel floor as depicted before in Figure IV-9. Care was taken to ensure all tufts were capable of full motion throughout the testing. The wind tunnel was activated and a flow mapping was made with no blower suction. The data acquisition system was manually started and pressure coefficients of the various surface ports were calculated according to Appendix A.

2. Suction Through a 2.5 Inch Diameter Hole

Two 2.5 inch diameter holes were drilled on both sides of the base platform at the location from Chapter III. After the wind tunnel was up to full speed, the suction was turned on. Flow patterns again were noted and mapped while pressure data was recorded. The blower suction was varied from full-closed to 100% capacity through increments of 10% in order to determine minimum suction for quiescent flow. Total quiescent flow was never achieved.

3. Suction with the Aft Area Covered

To obtain better results, two large L-shaped holes were cut out of the plywood on either side of the nosepiece. The holes could then be fitted with the two-piece adjustable

hole control or a porous plate (as shown before in Figure IV-10). For this part of the test, the aft portions of the hole control covered the area closest to the nosepiece. Suction was varied and data was recorded.

4. Suction with the Forward Area Covered

The same test as in part 3 above was conducted, but the forward portion of the hole was now the covered area.

5. Suction Through a 2 Inch Slot

Both pieces were then screwed to the base platform. A two inch slot was left directly in the center to determine suction performance. This test simulated moving a vortex "hole" out from the nosepiece area from where it was positioned previously in part 1. The location of the slot was varied in the general area with very little noticeable flow changes.

6. Suction Through the Porous Plate

Two porous aluminum plates were screwed over both base platform holes and similar tests were run. The porous plates were used to determine whether they would help or hinder the suction performance.

7. Suction Through Large Uncovered Holes

All covering plates were removed during the final testing. This proved to be the most optimum condition during the experimental research.

B. FLOW MAPPING RESULTS

To visualize the test flow patterns, figures were drawn using the tufts as guides. Tufts demonstrated three basic types of motion: smooth flow, mild turbulence, and very strong vorticity.

It was noticed during testing that turbulence would decrease when the suction was increased in steps. All cases examined never fully reached total quiescent flow.

1. No Suction

Figure VI-1 is a flow plot without suction through the base platform. Notice the extreme turbulence depicted by the vorticity arrows, which is typical of fully separated flow. There is an upflow from the 270 degree point at the base to the 210 degree point close to the top of the turret. The nosepiece is also directing airflow in an opposite direction downwards. The entire nosepiece and aft turret show disturbed flow at almost all locations.

2. Suction Through a 2.5 Inch Diameter Hole

A much quieter flow pattern can be seen along the nosepiece surface in Figure VI-2. Notice that the separation point has moved further aft. However, the lower portion of the turret is still very turbulent with opposing flow vectors. The results of this experiment forced the cutting of a larger suction area on both sides of the base platform.

3. Suction with the Aft Area Covered

Figure VI-3 illustrates the improved performance with a much larger suction hole in the base platform. Notice the aft hole area closest to the nosepiece is covered up by one part of the two-piece adjustable aluminum hole control. The turbulent vorticity at the turret base has ceased, but the flow is now more unsteady nearer the top as compared to Figure VI-2. The airflow at the bottom section of the nosepiece is forced towards the suction hole, causing increased disruption. Flow along the base platform is also being sucked through the hole.

4. Suction with the Forward Area Covered

When the forward portion of the suction hole is covered (Figure VI-4), there is a noticeable delay in separation around the lower base of the turret. Most of the tufts are lying flat in the direction of the suction hole. There is still some mild turbulence coming over the top aft portion of the turret and downwards in an "S" shaped path.

5. Suction Through a 2 Inch Slot

As noted before, this test was to simulate moving the vortex hole out from the nosepiece body. From Figure VI-5, it can be seen that the amount of airflow being drawn off is not enough to control separation. Various positioning of the flow control plates proved fruitless for quiescent flow patterns.

6. Suction Through the Porous Plate

Figure VI-6 depicts the porous plate covering the entire suction area. Notice that the upper aft portions of the turret still show mild turbulence while the separation point was moved to about the 225 degree position. The porous plate had a solidity of about 60%. It is interesting to note that the larger hole areas perform better even when the flow is reduced by a fixture such as a porous plate.

7. Suction Through Large Uncovered Holes

As was expected, the optimum performance was demonstrated with the maximum possible area open for suction. Figure VI-7 shows the best flow field in all the major runs. Notice, however, that total quiescent flow was never fully achieved during these tests. Increasing the suction rate would usually cause the turbulence to decrease at some points, but the design did not produce adequate performance.

C. PRESSURE COEFFICIENT RESULTS

Pressure coefficient values from section BB (Figure V-1) were calculated for various runs. The runs included: no suction, 50% suction through 2.5 inch diameter holes, 10% suction through large uncovered holes, and 50% suction through large uncovered holes. Pressure coefficient values from section BB were plotted because that section was the major region of turbulence for all test runs. Results were plotted against the theoretical surface pressure distribution

for a cylinder. Pressure taps at the 180 degree position were covered by the nosepiece, therefore those coefficients were not plotted. Figure VI-8 is a graph of the pressure coefficients for the various test runs compared to theory. Notice how increased suction and increased suction hole size demonstrate a pressure distribution close to the theoretical plot.

Table VI-1 gives a pressure coefficient distribution of the nine nosepiece ports during test runs. Recall that this area usually showed very calm flow conditions.

VII. CONCLUSIONS AND RECOMMENDATIONS

A. CONCLUSIONS

The use of the nosepiece design with suction generally improved flow conditions over the laser turret. However, total quiescent flow was never fully achieved during all test cases. Increased suction port area in the base platform permitted better flow performance.

The nosepiece design was not capable of stabilizing shed vortices. Most test cases with suction demonstrated smooth flow over the top of the turret.

Based on the calculations conducted during design, the computer model was not an effective tool for flow prediction. The nosepiece design requires more accurate information for construction due to its complexity.

B. RECOMMENDATIONS

The idea of stabilized vortices for blunt body flow control should not be discounted. A more adequate three dimensional computer model is needed to fulfill design requirements. A vorticity measuring device would help to determine strength and location of trapped vortices.

APPENDIX A
EVALUATION OF THE PRESSURE COEFFICIENT

Another form of turret flow performance can be determined by using the following equation

$$\frac{p_s - p_\infty}{\frac{1}{2}\rho U^2} = \frac{\Delta p}{q} \quad (A-1)$$

where $\frac{\Delta p}{q}$ is called the pressure coefficient (C_p). The value p_s is the static pressure at the point of interest measured from the turret or nosepiece taps. The static pressure in the wind tunnel is p_∞ and the freestream dynamic pressure is q . The difference between wind tunnel total pressure (p_D) and wind tunnel static pressure (p_∞) determine q . In other words, equation (A-1) can be expressed as

$$C_p = \frac{\Delta p}{q} = \frac{p_s - p_\infty}{p_D - p_\infty} \quad (A-2)$$

Since the pressure coefficient is non-dimensional, values obtained from the teletype can be directly entered into equation (A-2) without using a "centimeters of water" conversion.

TABLE III-1
 COORDINATES OF INITIAL PANEL DESIGN
 (From Figure III-5)

POINT NUMBER	X, Y COORDINATES
1	(0, 0)
2	(0.134, 0.5)
3	(0.5, 0.866)
4	(1.0, 1.0)
5	(1.5, 0.866)
6	(2.119, 0.625)
7	(2.387, 0.625)
8	(2.452, 0.417)
9	(2.774, 0.286)
10	(2.940, 0.327)
11	(3.071, 0.4762)
12	(3.131, 0.625)
13	(3.25, 0.625)
14	(3.488, 0.625)
15	(8.964, 0.625)
16	(11.375, 0)
17	(8.964, -0.625)
18	(3.488, -0.625)
19	(3.25, -0.625)

TABLE III-1 (Continued)

POINT NUMBER	X, Y COORDINATES
20	(3.131, -0.625)
21	(3.071, -0.4762)
22	(2.940, -0.327)
23	(2.774, -0.286)
24	(2.452, -0.417)
25	(2.387, -0.625)
26	(2.119, -0.625)
27	(1.5, -0.866)
28	(1, -1)
29	(0.5, -0.866)
30	(0.134, -0.5)

TABLE III-2
COORDINATES OF NOSEPIECE VARIATIONS
(From Figure III-6)

POINT NUMBER	X, Y COORDINATES
6	(2.119, 0.119)
7	(2.446, 0.149)
8	(2.773, 0.179)
9	(2.982, 0.25)
10	(3.101, 0.327)
11	(3.191, 0.446)
12	(3.190, 0.625)
20	(3.190, -0.625)
21	(3.191, -0.446)
22	(3.101, -0.327)
23	(2.982, -0.25)
24	(2.773, -0.179)
25	(2.446, -0.149)
26	(2.119, -0.119)

TABLE III-2 (Continued)

(From Figure III-7)

POINT NUMBER	X,Y COORDINATES
6	(2.119, 0.298)
7	(2.625, 0.179)
8	(2.893, 0.119)
9	(3.042, 0.155)
10	(3.131, 0.250)
11	(3.160, 0.381)
12	(2.982, 0.607)
20	(2.982, -0.607)
21	(3.160, -0.381)
22	(3.131, -0.250)
23	(3.042, -0.155)
24	(2.893, -0.119)
25	(2.625, -0.179)
26	(2.119, -0.298)

(From Figure III-8)

POINT NUMBER	X,Y COORDINATES
6	(2.00, 0.369)
7	(2.357, 0.357)
8	(2.625, 0.149)

TABLE III-2 (Continued)

(From Figure III-8)

POINT NUMBER	X, Y COORDINATES
9	(2.833, 0.167)
10	(3.012, 0.286)
11	(3.131, 0.446)
12	(3.190, 0.625)
20	(3.190, -0.625)
21	(3.131, -0.446)
22	(3.012, -0.286)
23	(2.833, -0.167)
24	(2.625, -0.149)
25	(2.357, -0.357)
26	(2.00, -0.369)

TABLE III-3
COORDINATES OF FINAL PANEL DESIGN

POINT NUMBER	X, Y COORDINATES
1	(0,0)
2	(0.134, 0.5)
3	(0.5, 0.866)
4	(1.0, 1.0)
5	(1.5, 0.866)
6	(2.119, 0.298)
7	(2.30, 0.173)
8	(2.55, 0.119)
9	(2.65, 0.155)
10	(2.73, 0.250)
11	(2.75, 0.381)
12	(2.68, 0.607)
13	(2.83, 0.625)
14	(3.070, 0.625)
15	(8.547, 0.625)
16	(10.958, 0.0)
17	(8.547, -0.625)
18	(3.070, -0.625)
19	(2.83, -0.625)
20	(2.68, -0.607)

TABLE III-3 (Continued)

POINT NUMBER	X, Y COORDINATES
21	(2.75, -0.381)
22	(2.73, -0.250)
23	(2.65, -0.155)
24	(2.55, -0.119)
25	(2.30, -0.179)
26	(2.119, -0.298)
27	(1.5, -0.866)
28	(1.0, -1.0)
29	(0.5, -0.866)
30	(0.134, -0.5)

TABLE III-4.
TANGENTIAL VELOCITIES AND PRESSURE
COEFFICIENTS OF FINAL PANEL DESIGN

PANEL (between points)	TANGENTIAL VELOCITIES	PRESSURE COEFFICIENTS
1, 2	0.495	0.755
2, 3	1.339	-0.794
3, 4	1.783	-2.178
4, 5	1.650	-1.723
5, 6	0.787	0.380
6, 7	-0.230	0.947
7, 8	-0.544	0.704
8, 9	-0.194	0.963
9, 10	-0.081	0.994
10, 11	-0.145	0.979
11, 12	-0.0	1.00
12, 13	1.347	-0.814
13, 14	1.117	-0.249
14, 15	1.092	-0.192
15, 16	1.037	-0.074
16, 17	-1.037	-0.074
17, 18	-1.092	-0.192
18, 19	-1.117	-0.249

TABLE III-4 (Continued)

PANEL (between points)	TANGENTIAL VELOCITIES	PRESSURE COEFFICIENTS
19, 20	-1.347	-0.814
20, 21	0.0	1.00
21, 22	-0.145	0.979
23, 23	-0.081	0.994
23, 24	-0.194	0.963
24, 25	-0.544	0.704
25, 26	-0.230	0.947
26, 27	-0.787	0.380
27, 28	-1.650	-1.723
28, 29	-1.783	-2.178
29, 30	-1.339	-0.794
30, 1	-0.495	0.755

TABLE VI-1
 PRESSURE COEFFICIENTS OF NOSEPIECE
 (Tap Locations from Figure V-2)

PRESSURE TAP LOCATION	NO SUCTION	SUCTION 2.5" HOLE	10% SUCTION LARGE HOLE	50% SUCTION LARGE HOLE
1	0.55	1.68	0.17	-0.20
2	0.36	0.62	0.35	0.06
3	0.58	0.72	0.52	0.29
4	-0.34	-0.63	-0.67	-1.67
5	-0.13	0.18	-0.52	-1.75
6	-0.54	0.31	-0.33	-1.49
7	0.37	-3.04	-3.21	-6.71
8	0.41	-2.18	-2.14	-4.62
9	0.38	-2.10	-1.36	-3.81

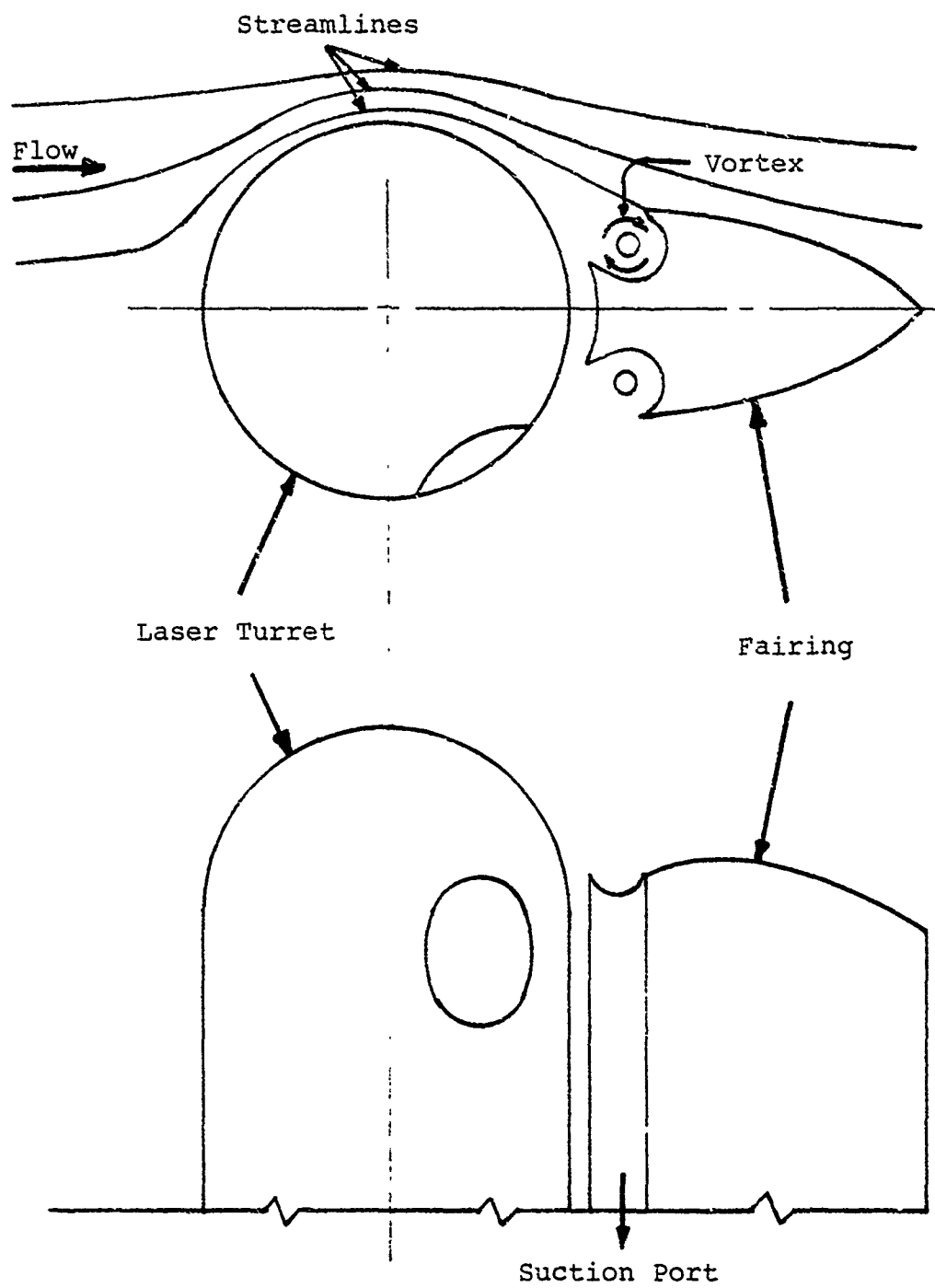
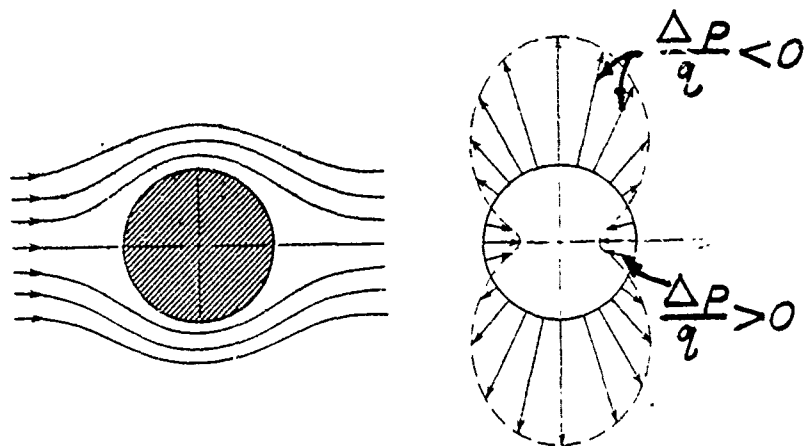
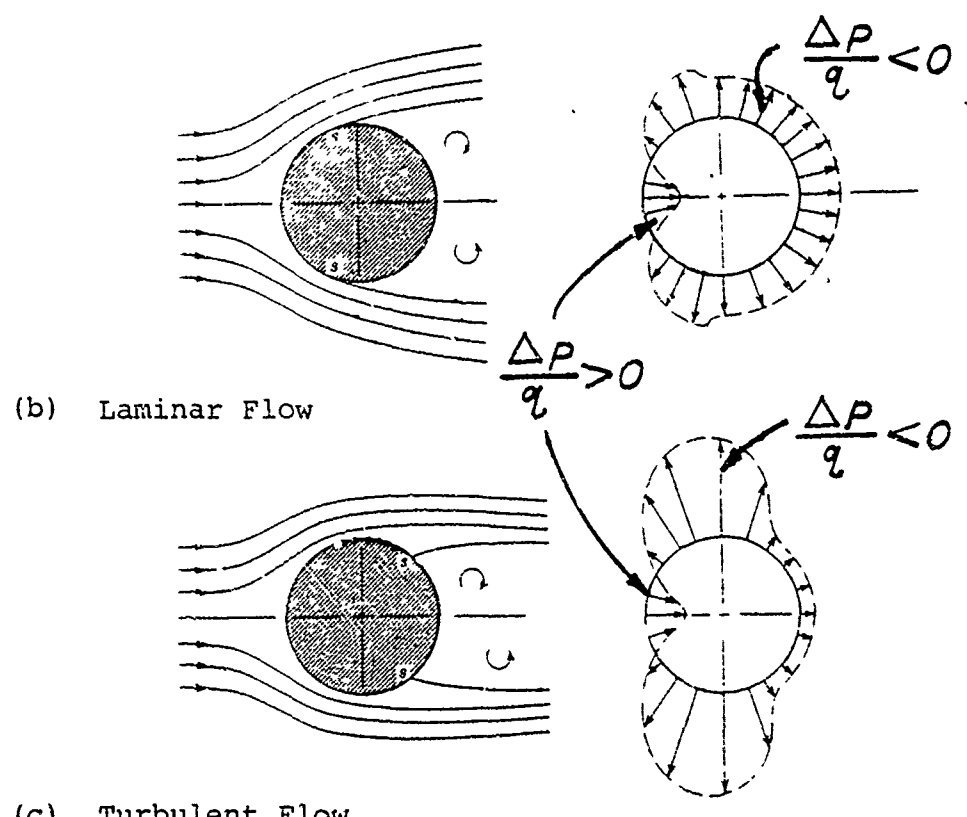


FIGURE I-1. TRAPPED VORTEX/SUCTION FAIRING,
FROM CRAIG [Ref. 6]



(a) Non Viscous Flow



(b) Laminar Flow

(c) Turbulent Flow

FIGURE II-1. FROM PAO [Ref. 5], STREAMLINE FLOW AND DISTRIBUTION FOR A CYLINDER

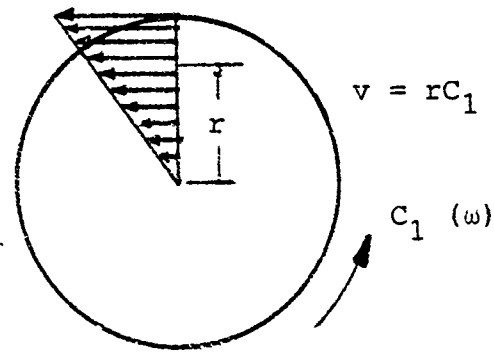


FIGURE II-2. VELOCITY DISTRIBUTION OF A FORCED VORTEX

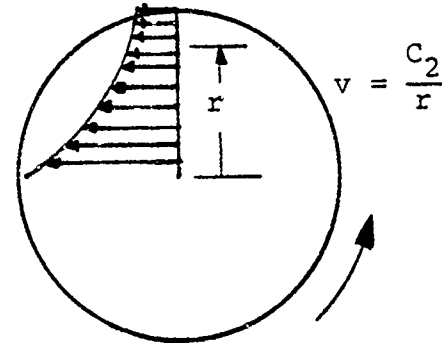


FIGURE II-3. VELOCITY DISTRIBUTION OF A FREE VORTEX

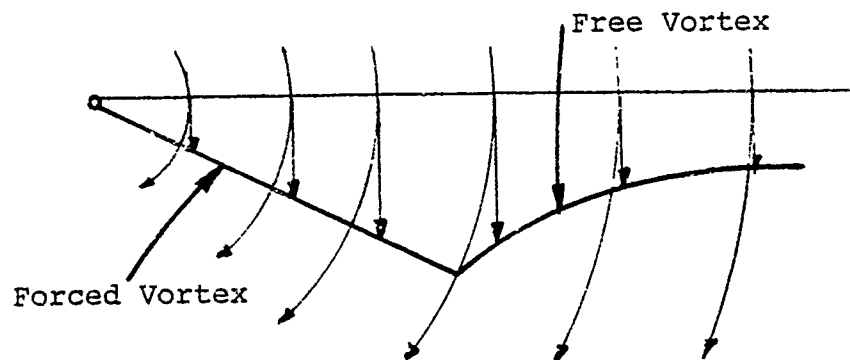


FIGURE II-4. VELOCITY DISTRIBUTION OF A RANKINE COMBINED VORTEX

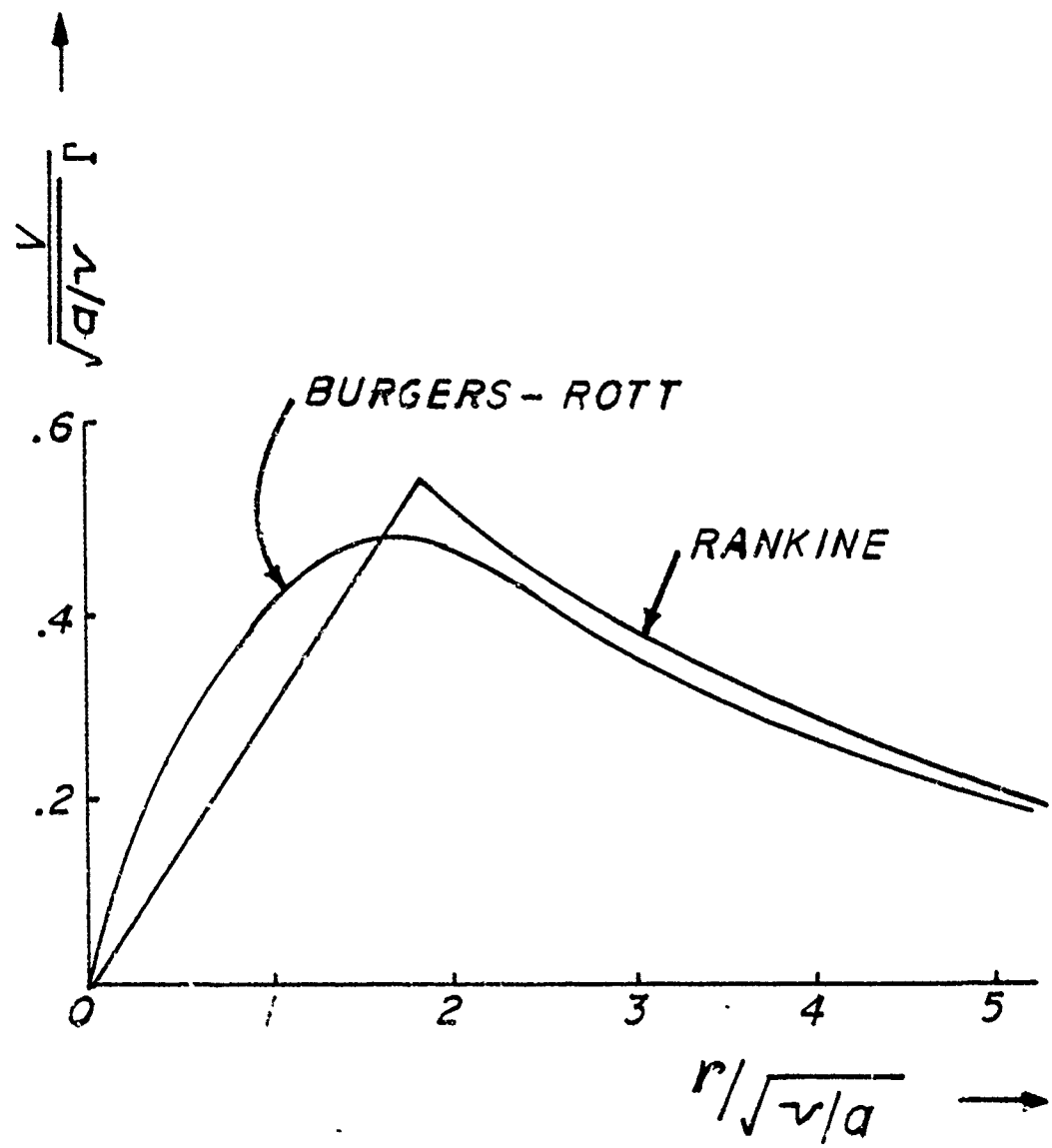


FIGURE II-5. NORMALIZED GRAPH OF THE BURGERS-ROTT AND RANKINE VELOCITY DISTRIBUTIONS

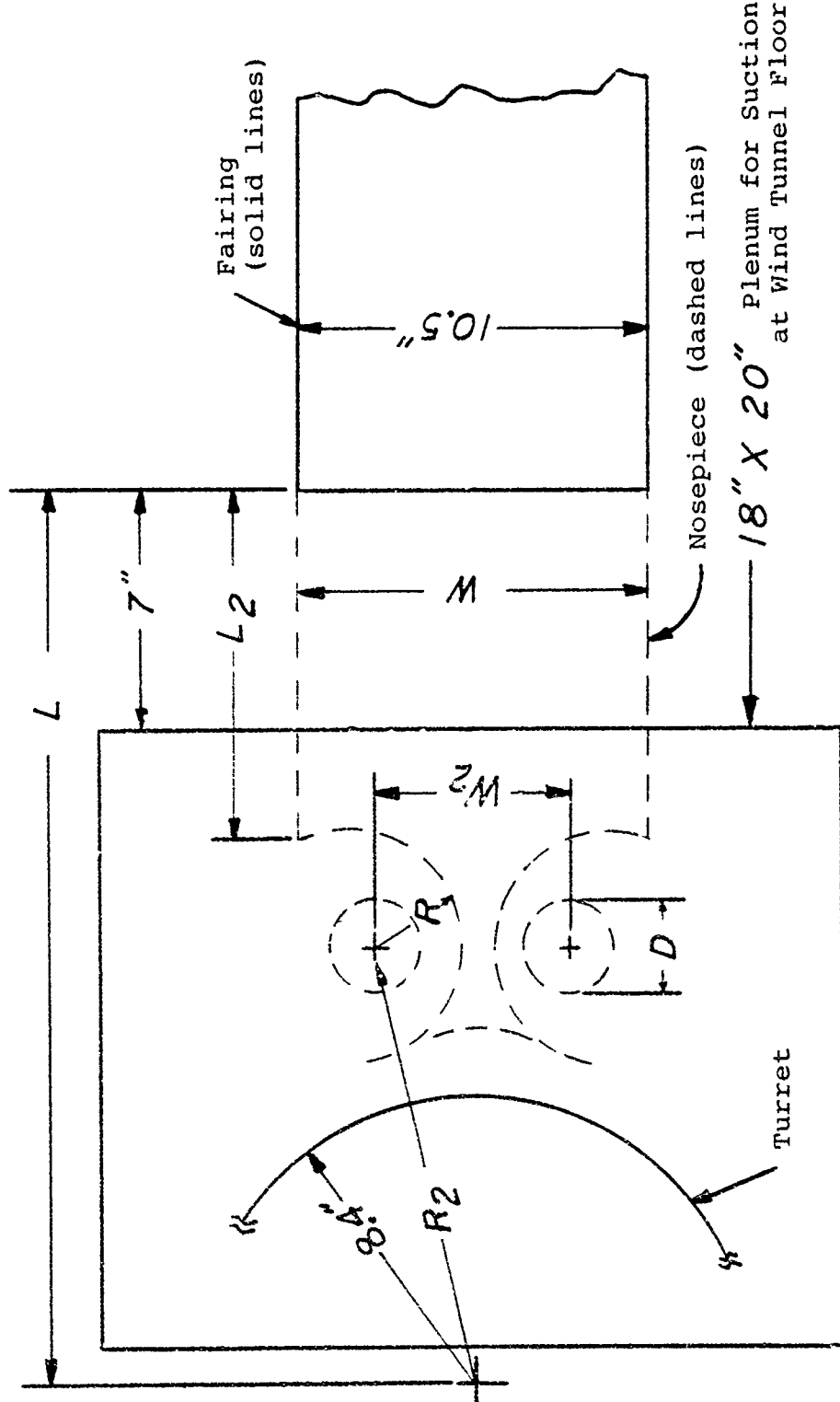


FIGURE III-1. FIXED AND VARIABLE GEOMETRIC PARAMETERS OF COMPONENTS (TOP VIEW LOOKING DOWN)

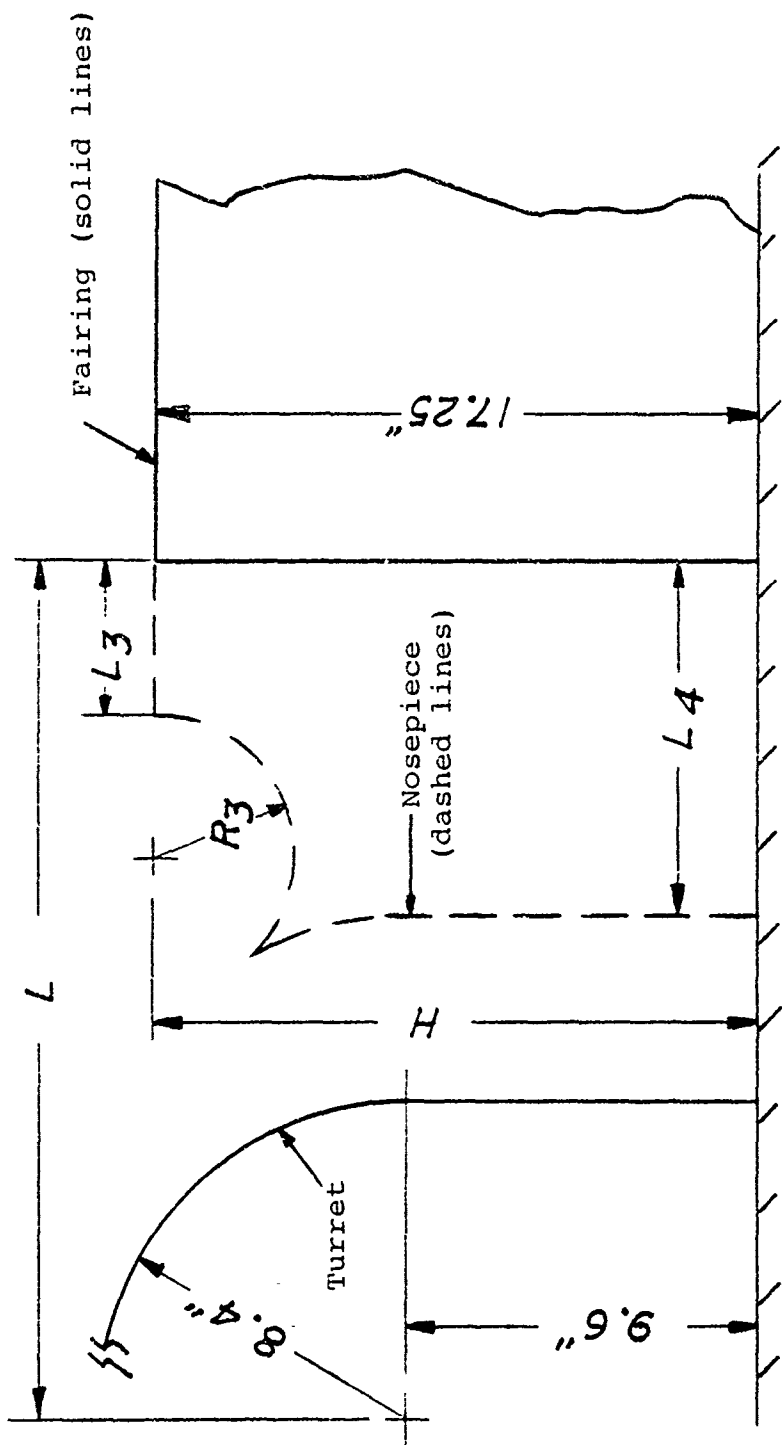


FIGURE III-2. SIDE VIEW OF COMPONENTS WITH FIXED AND VARIABLE GEOMETRIC PARAMETERS

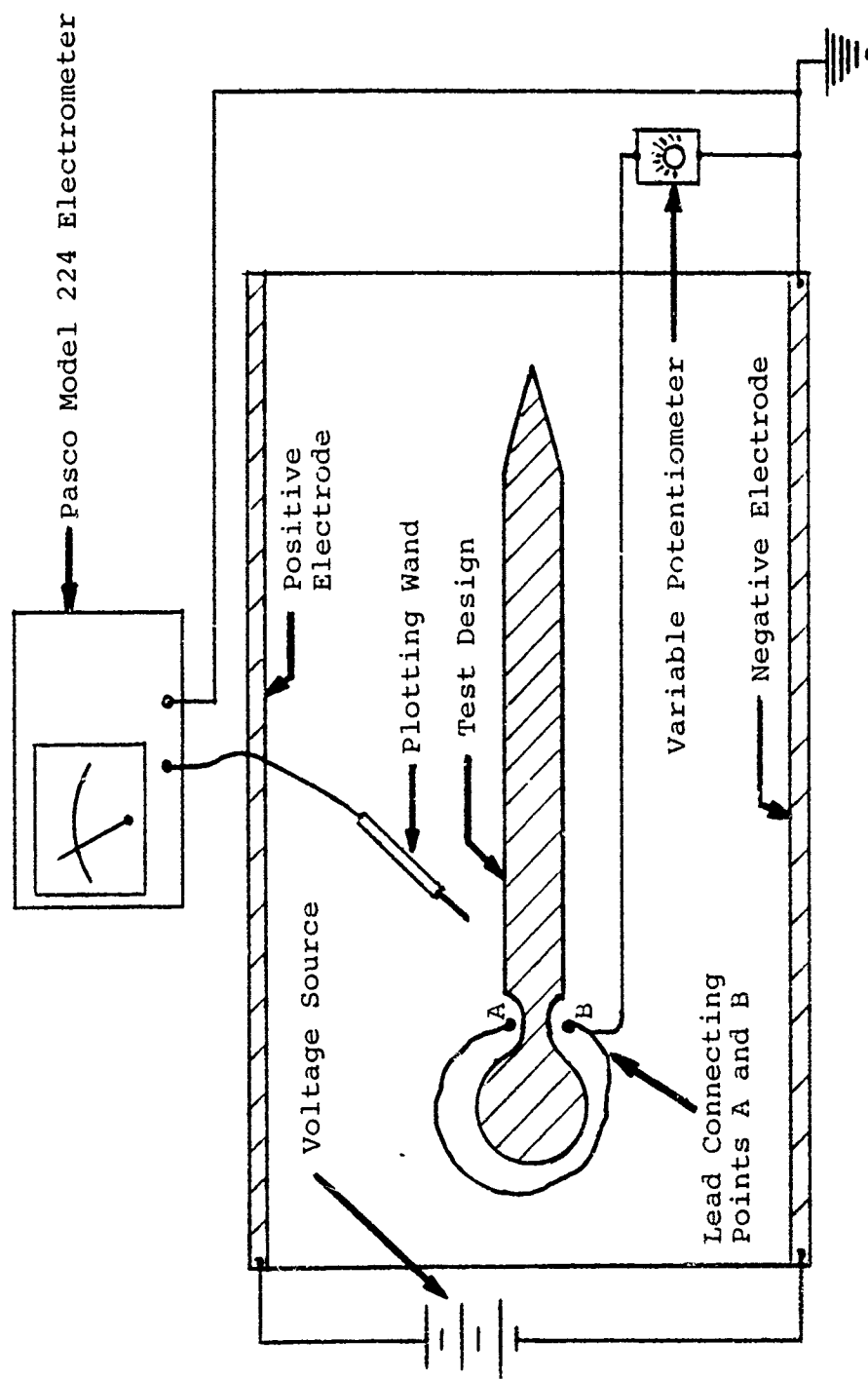


FIGURE III-3. TEST SETUP FOR EQUIPOTENTIAL PLOTTING

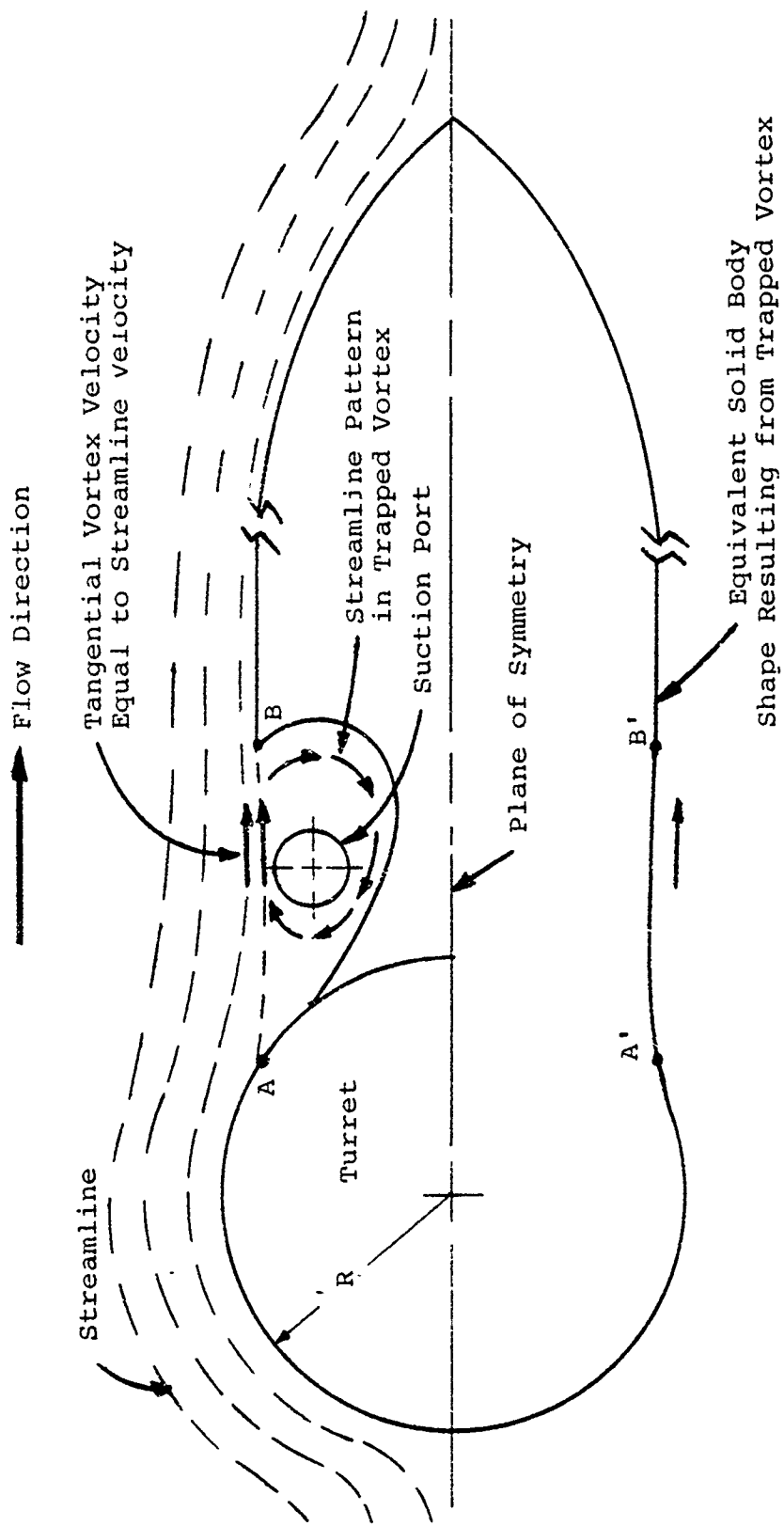


FIGURE III-4. DESIGN PHILOSOPHY FOR MATCHED VORTEX AND STREAMLINE FLOW

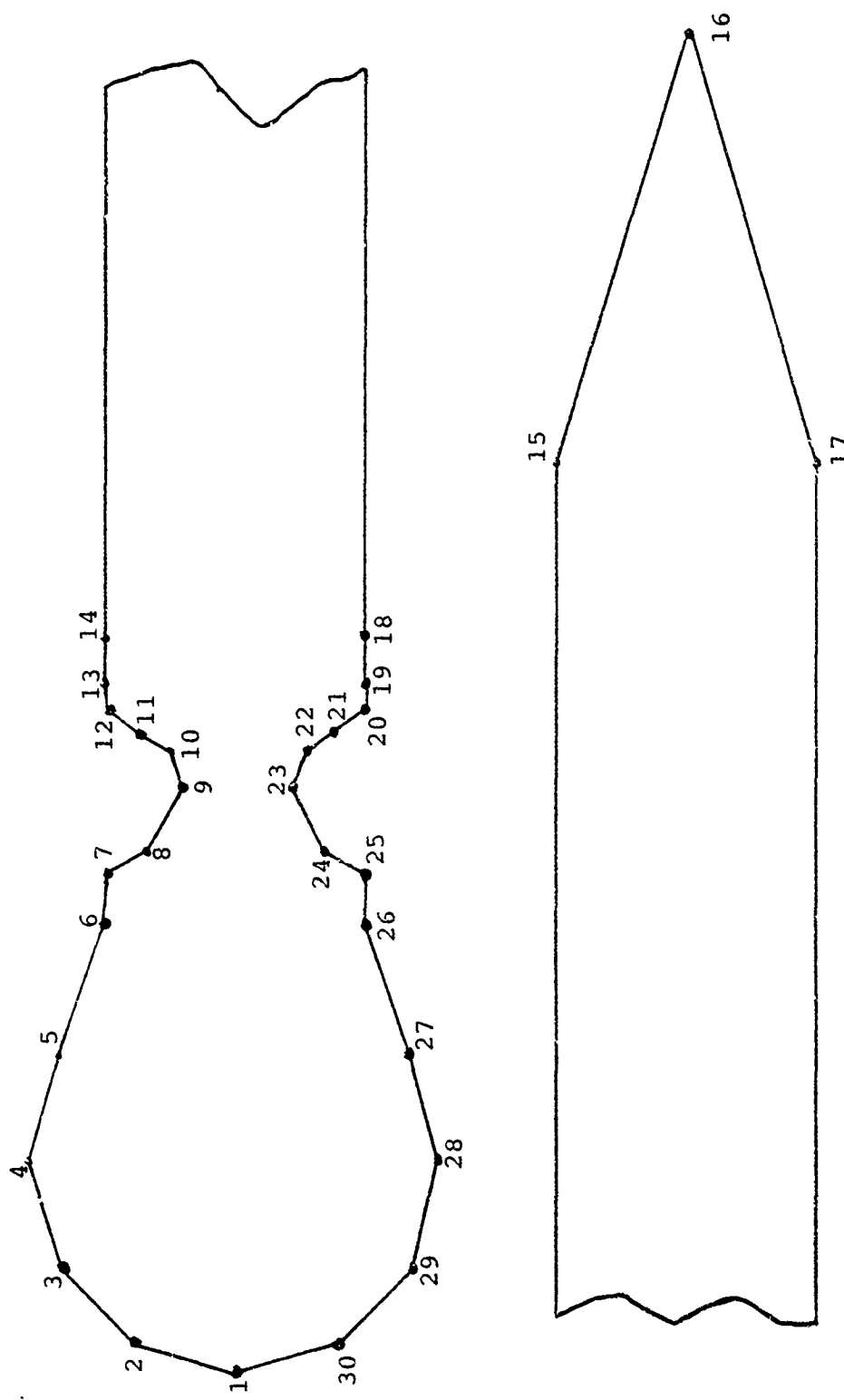


FIGURE III-5. INITIAL PANEL DESIGN

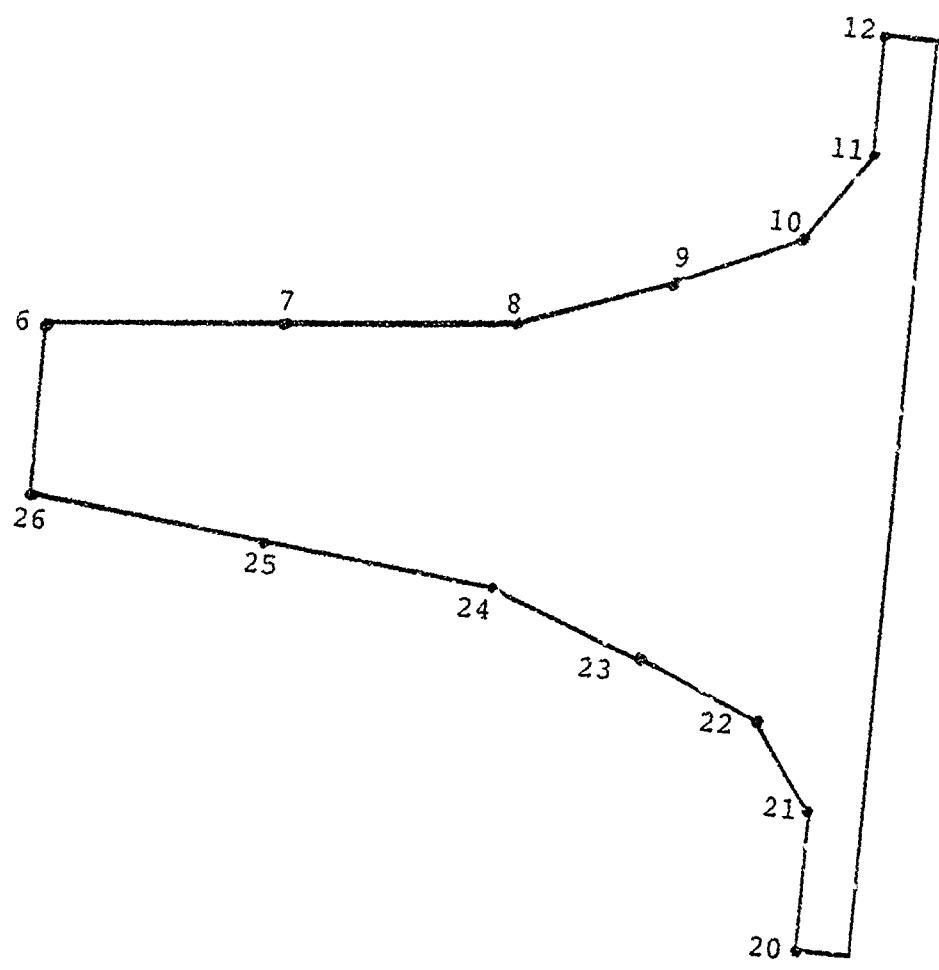


FIGURE III-6. FIRST NOSEPIECE DESIGN VARIATION

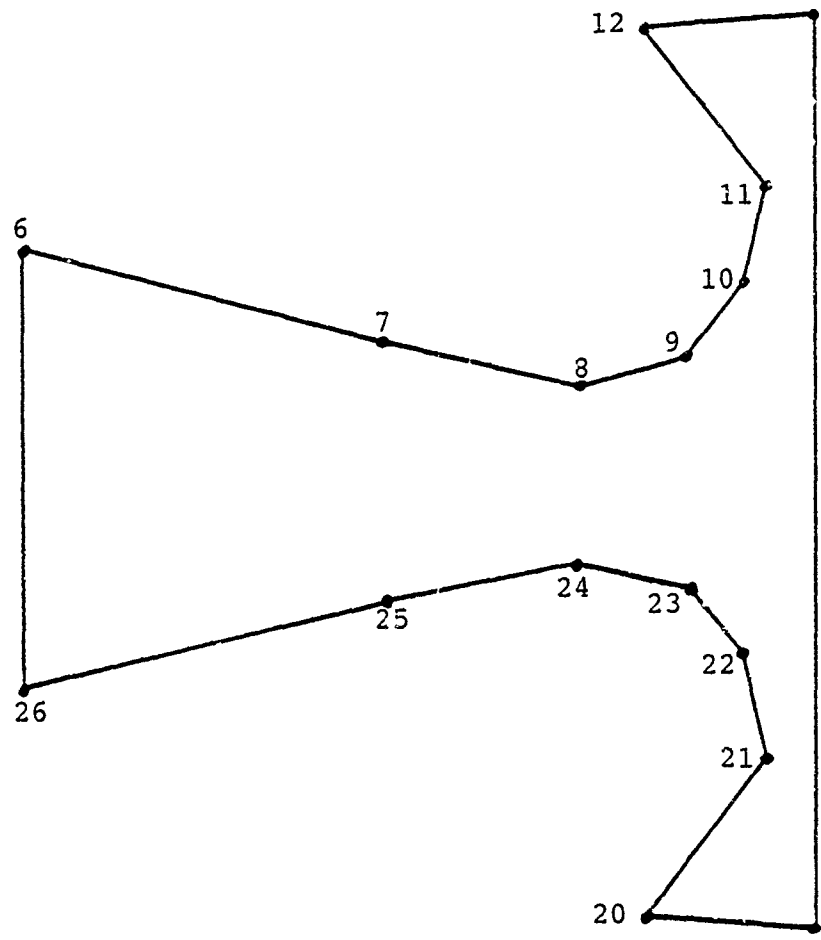


FIGURE III-7. SECOND NOSEPIECE DESIGN VARIATION

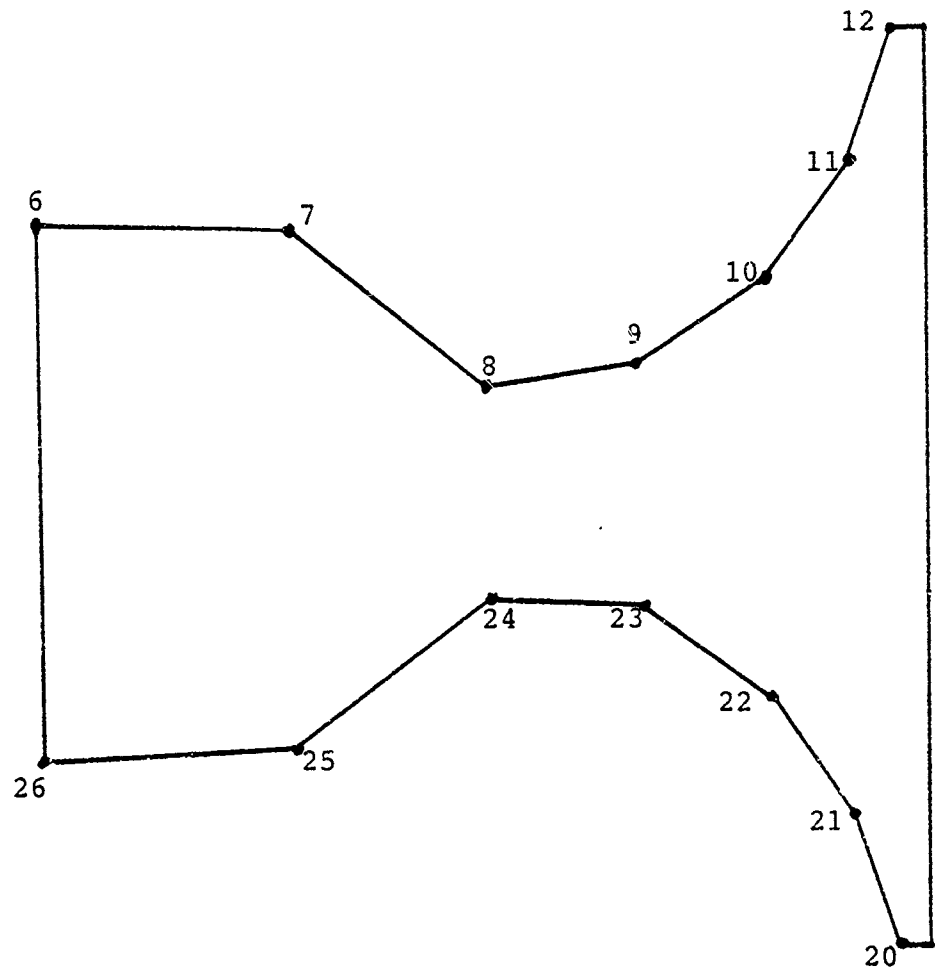


FIGURE III-8. THIRD NOSEPIECE DESIGN VARIATION

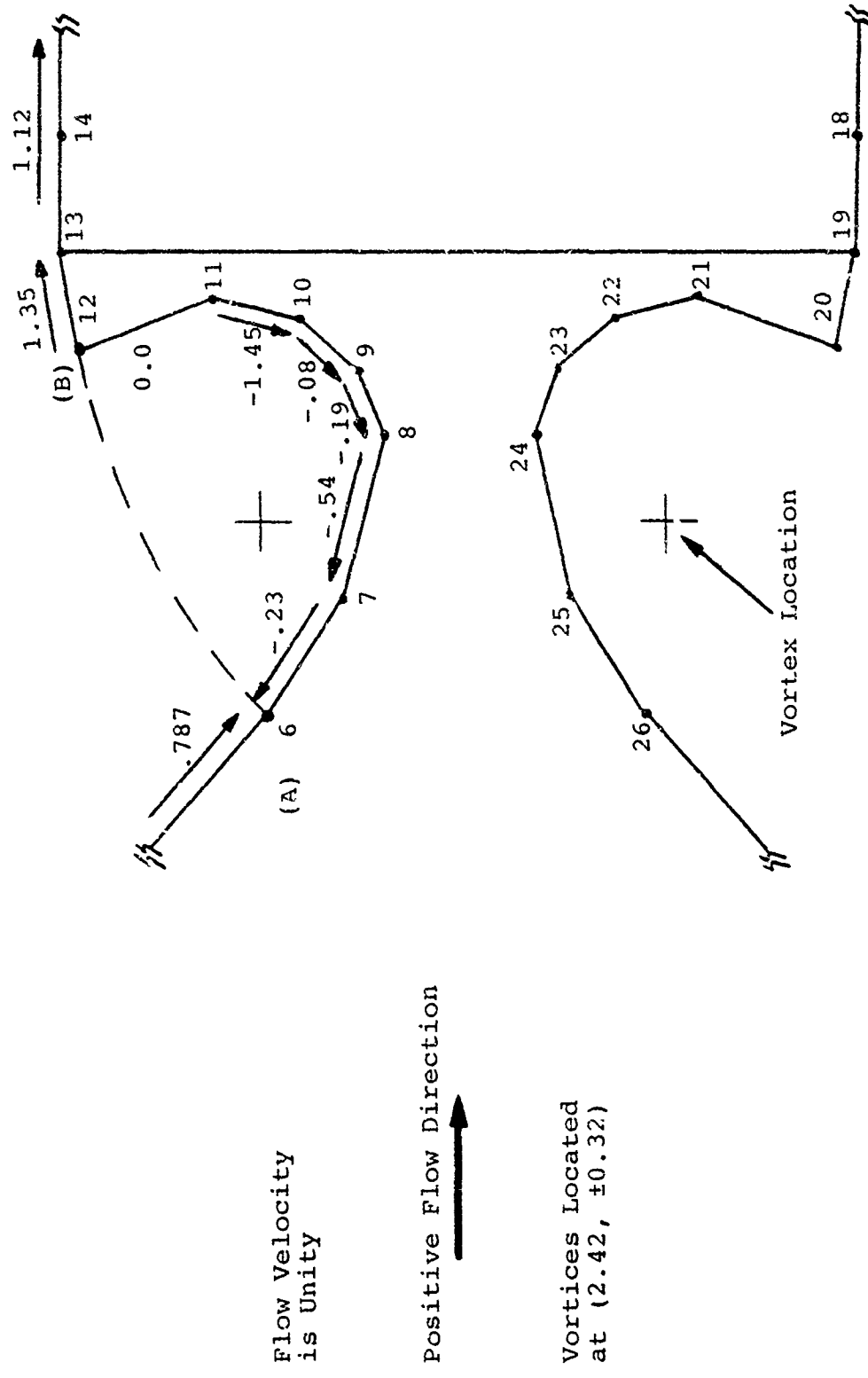


FIGURE III-9. TANGENTIAL VELOCITY PLOT

FIGURE III-10. COMPLETED DESIGN, SIDE VIEW

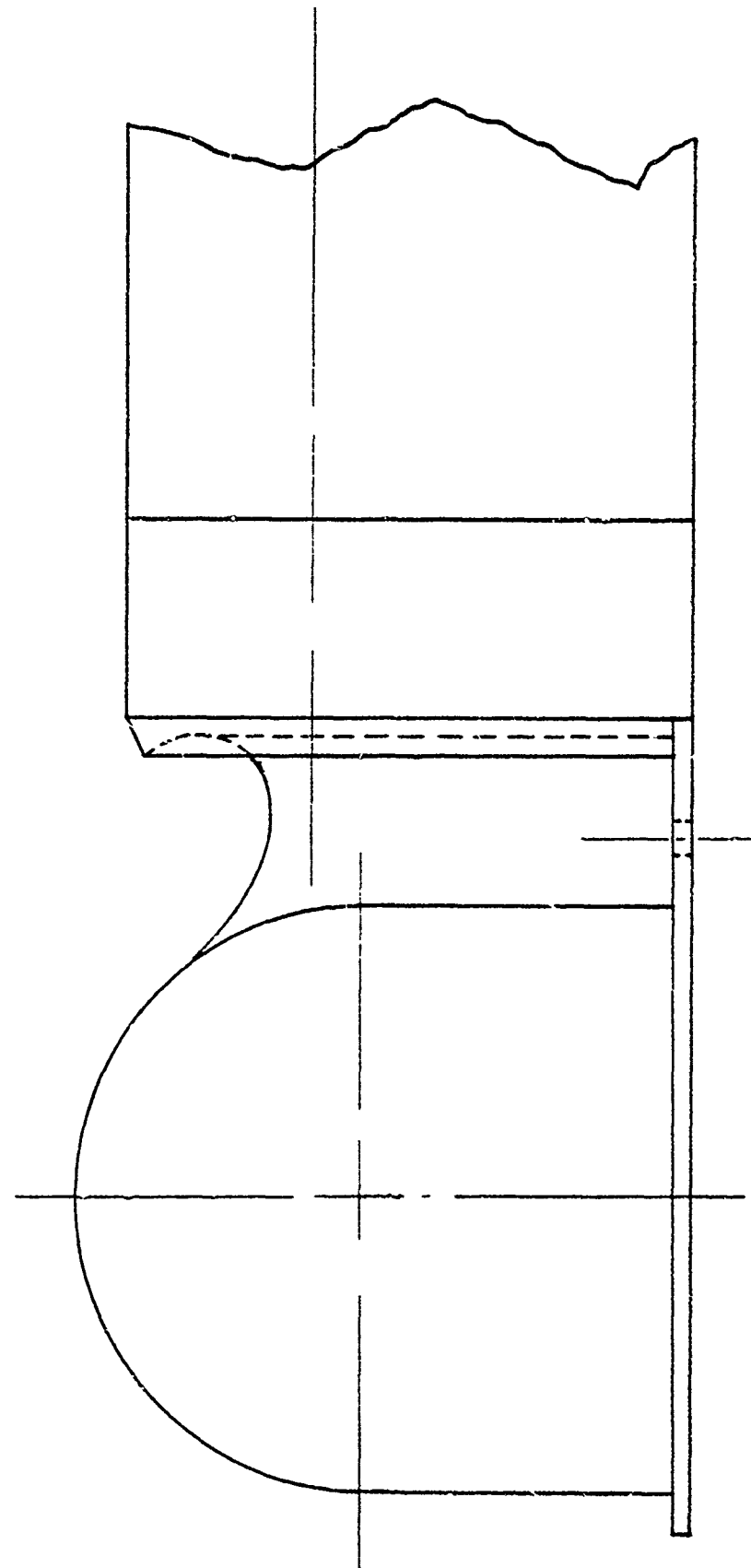


FIGURE III-11. COMPLETED DESIGN, TOP VIEW

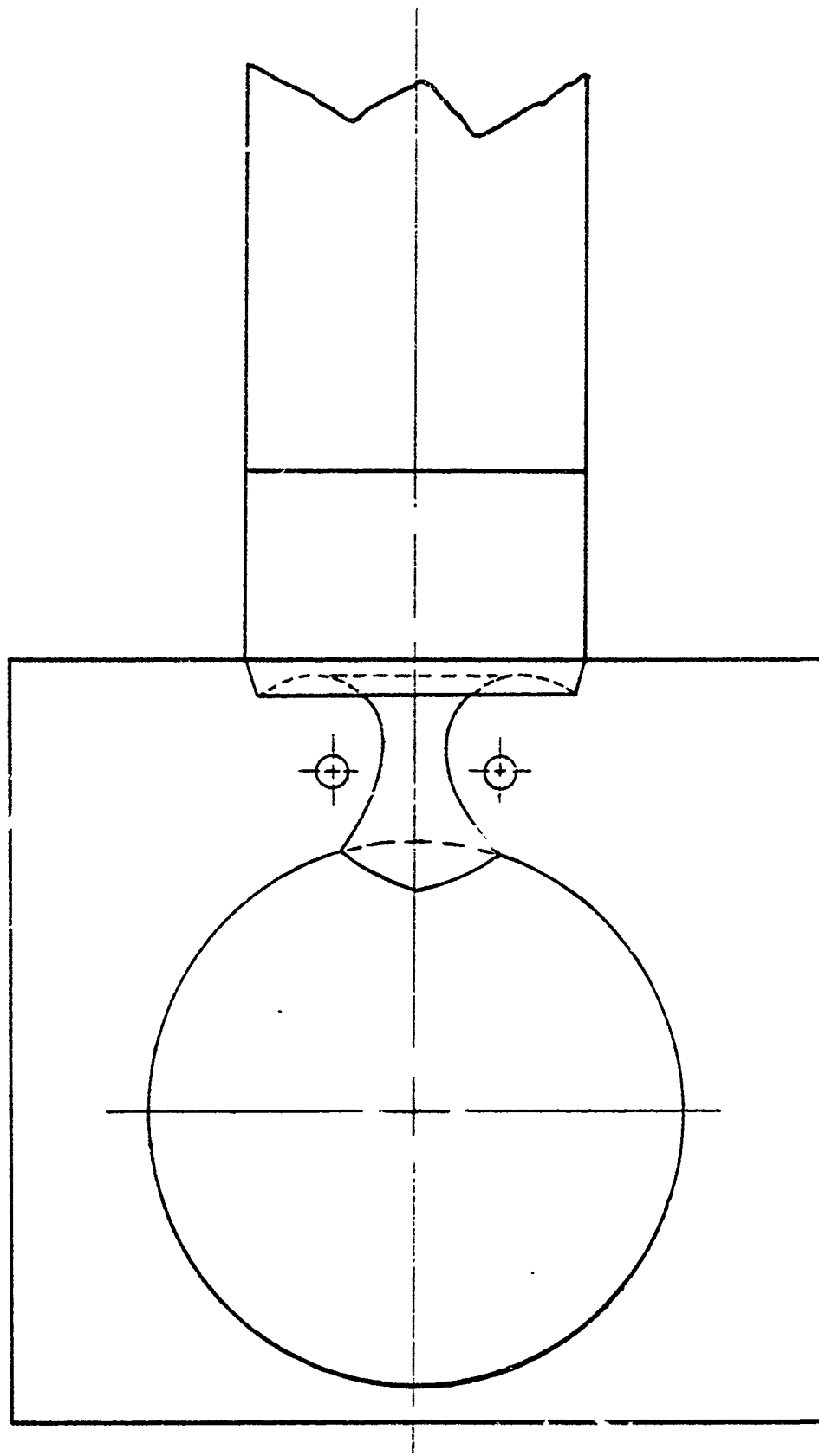


FIGURE III-12. COMPLETED DESIGN, END VIEW

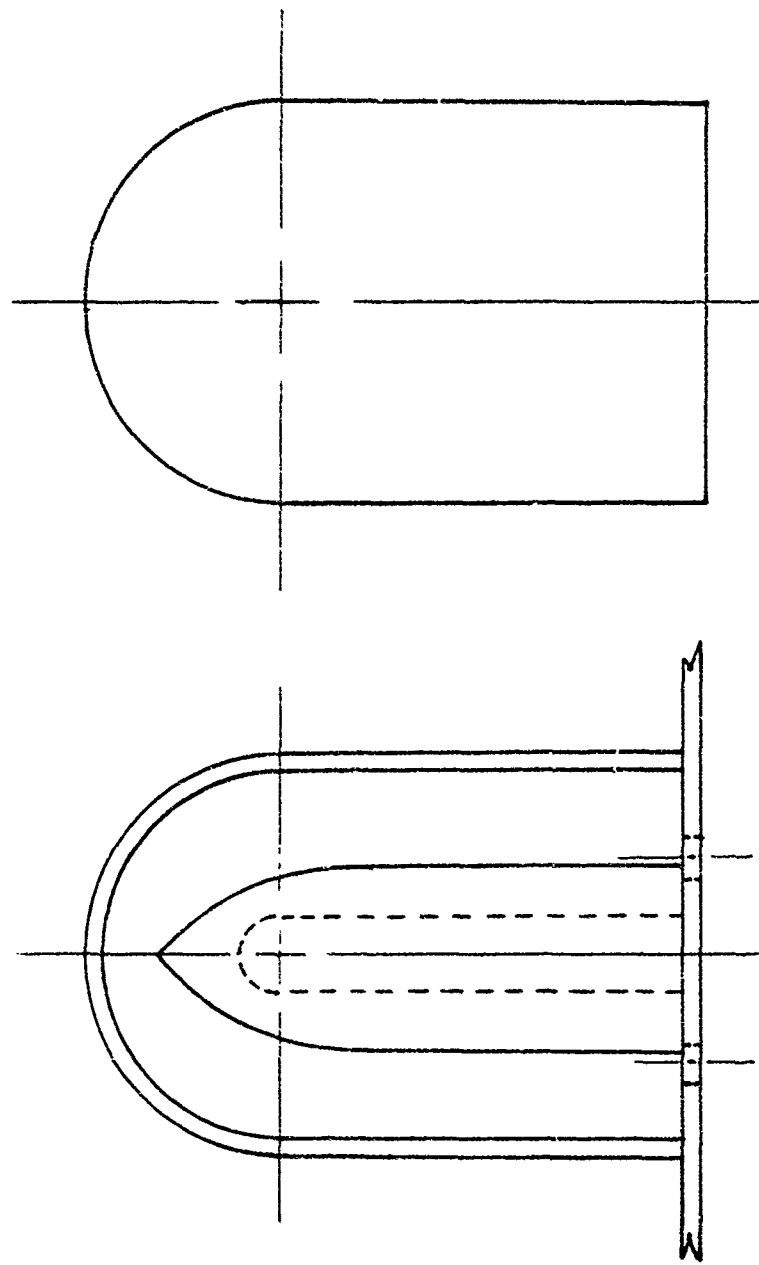
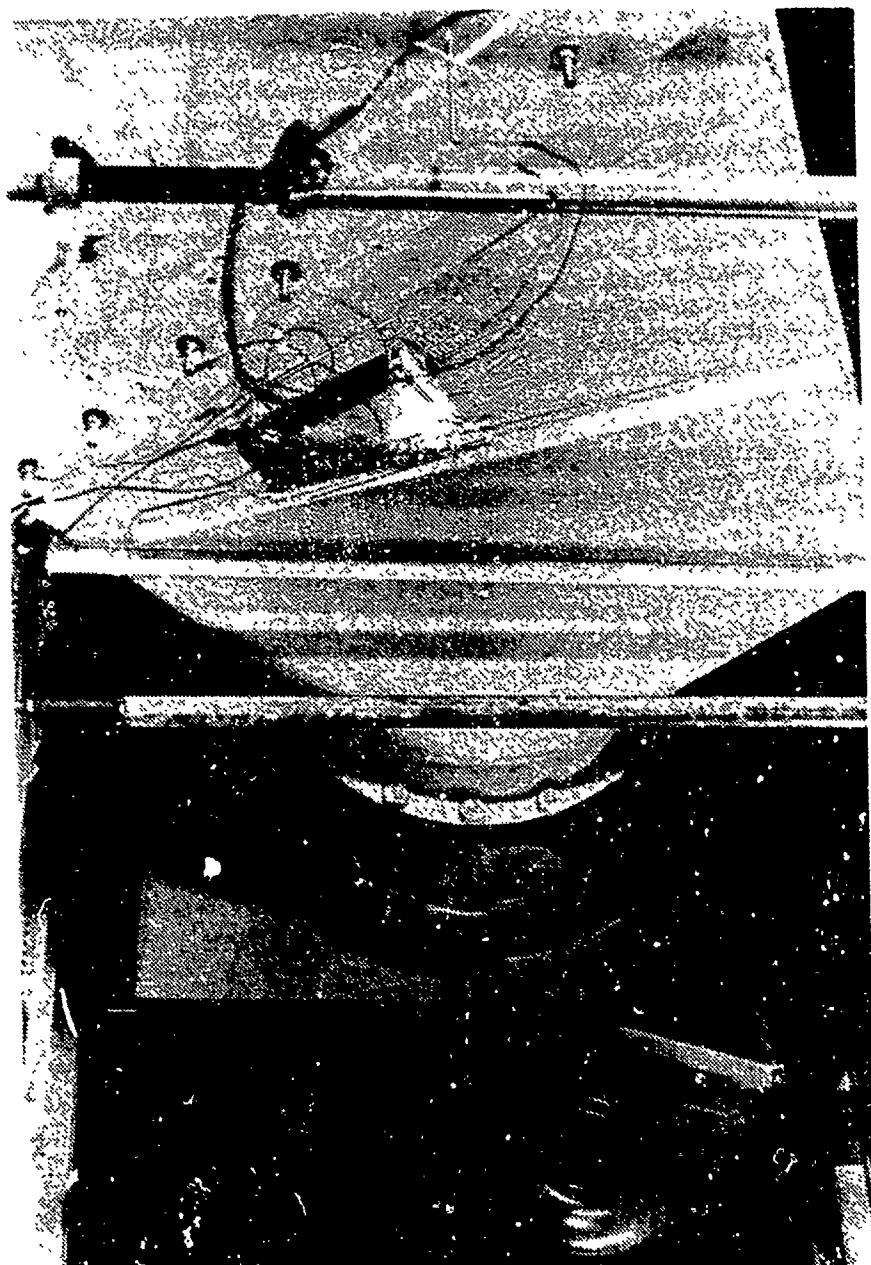


FIGURE IV-1. BLOWER AND DUCTWORK UNDERNEATH TUNNEL.



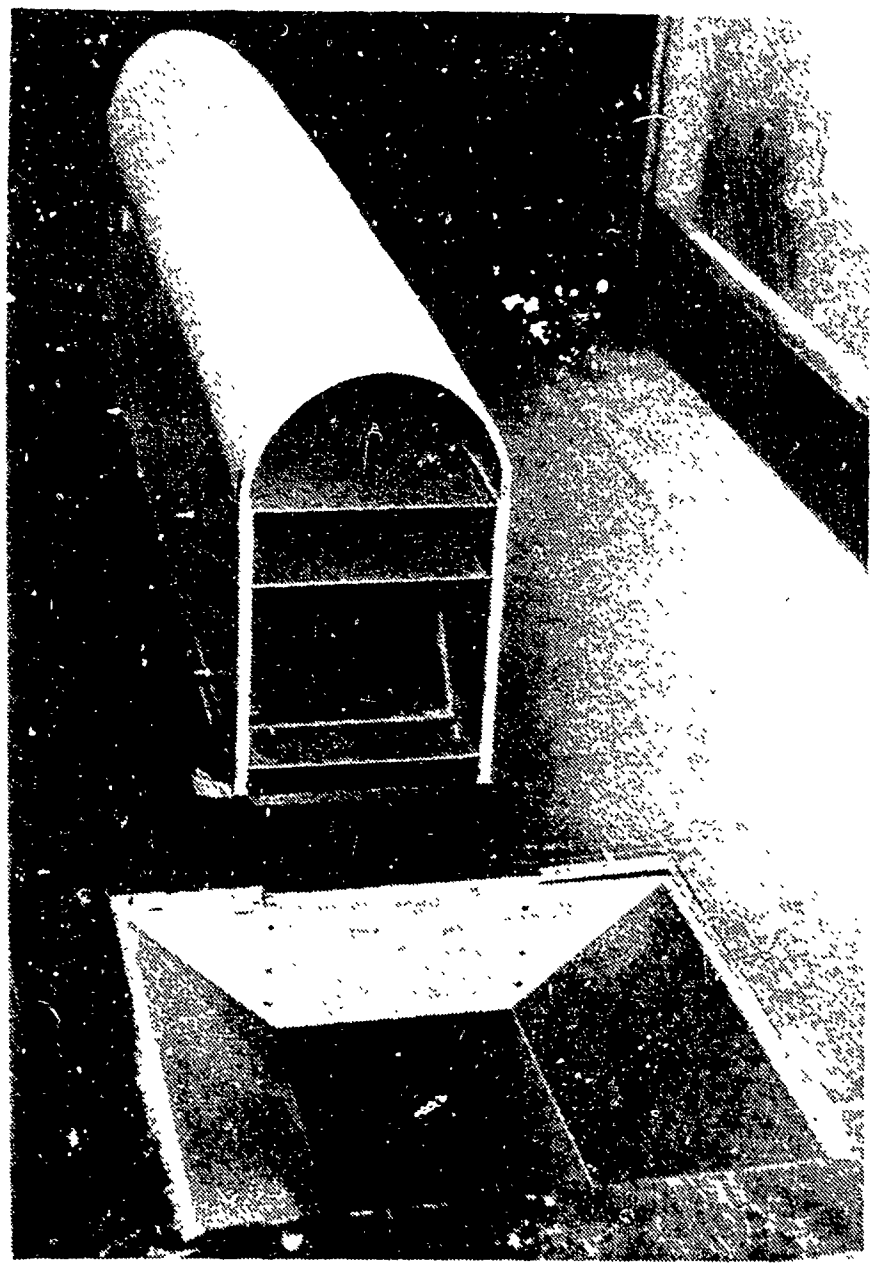


FIGURE IV-2. PLENUM CHAMBER AND FAIRING
(NOSEPIECE AND TURRET REMOVED)

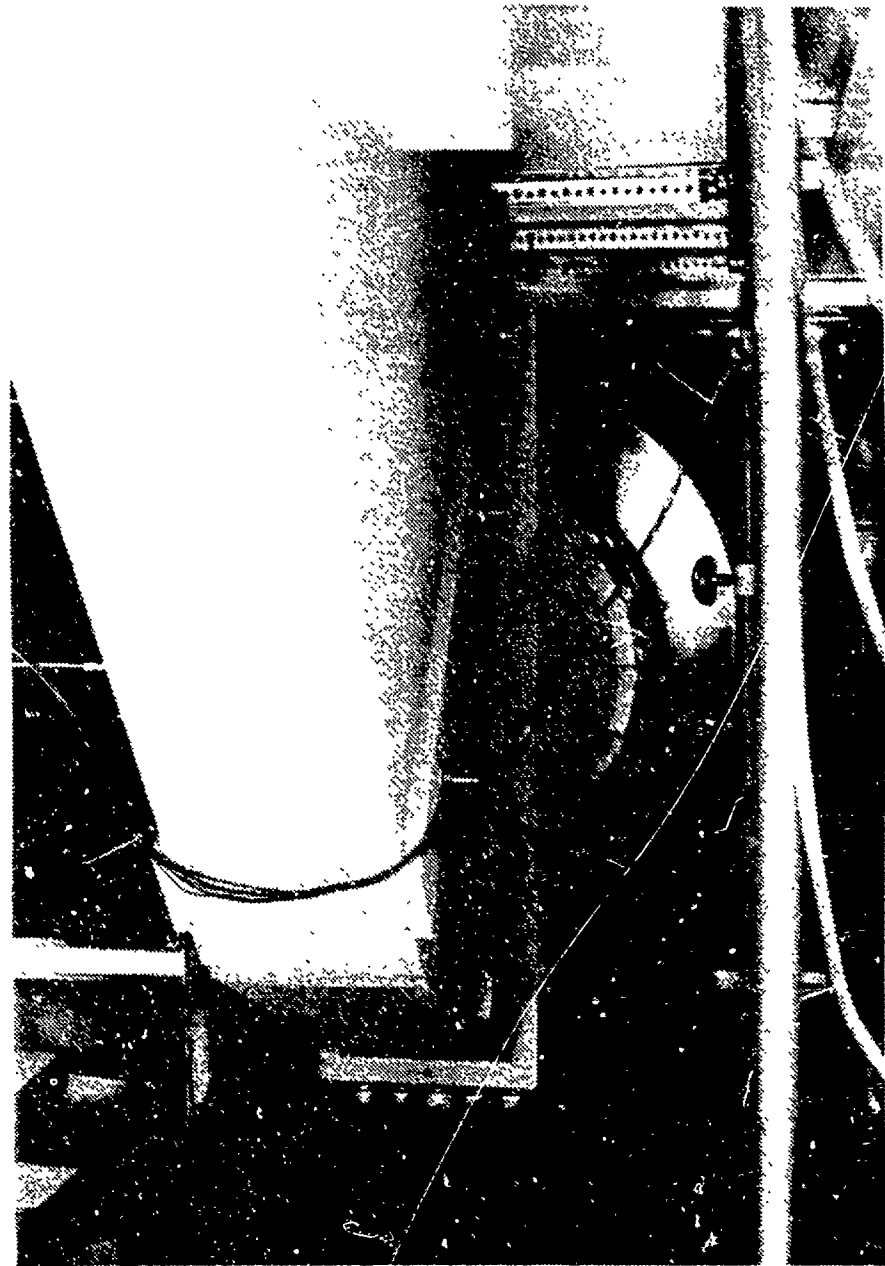


FIGURE IV-3. BLOWER AND DUCTWORK, BACK SIDE

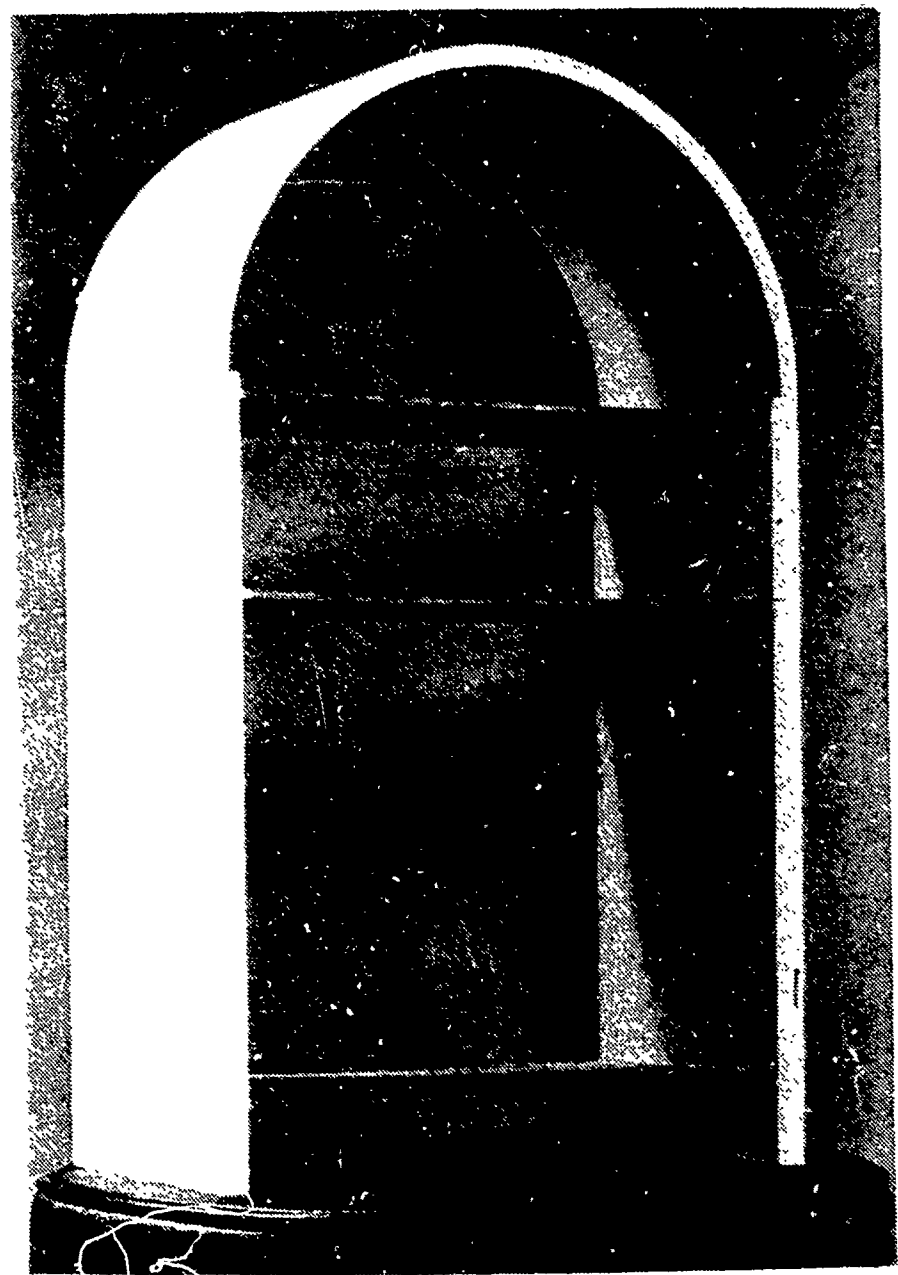


FIGURE IV-4. FILLER PIECE CONSTRUCTION

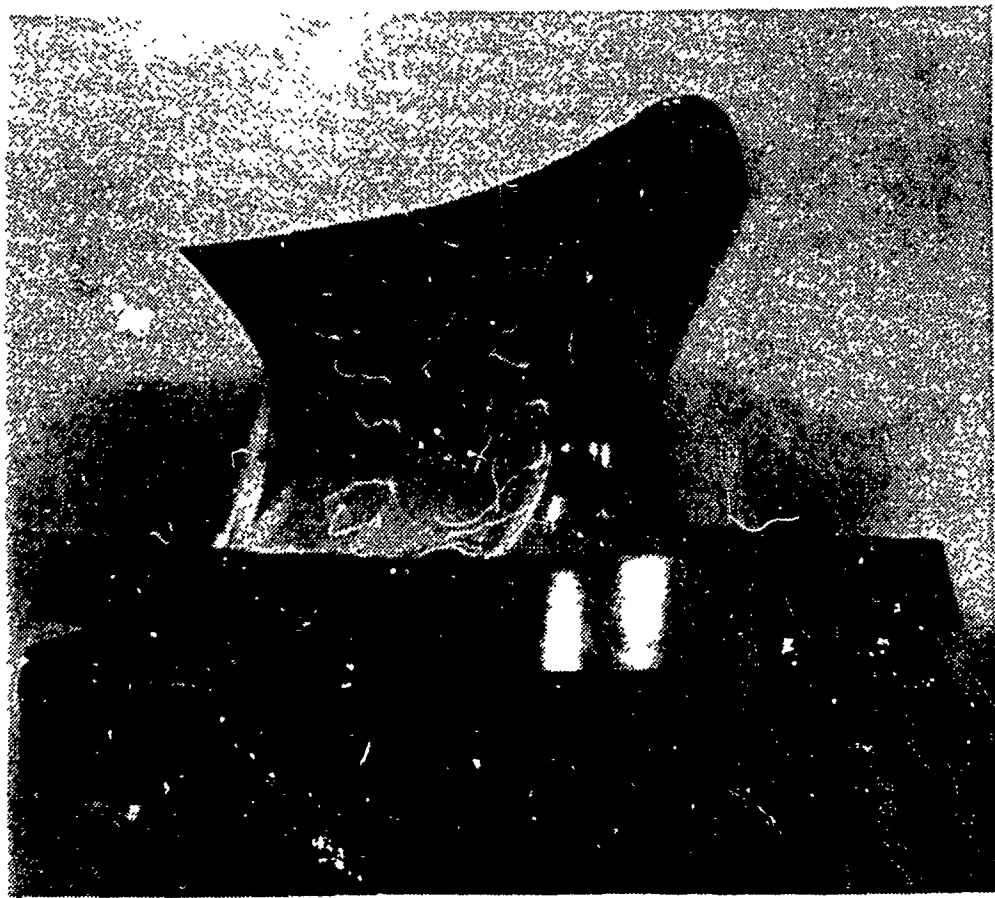


FIGURE IV-5. NOSEPIECE, TOP VIEW

FIGURE IV-6. NOSEPIECE, SIDE VIEW

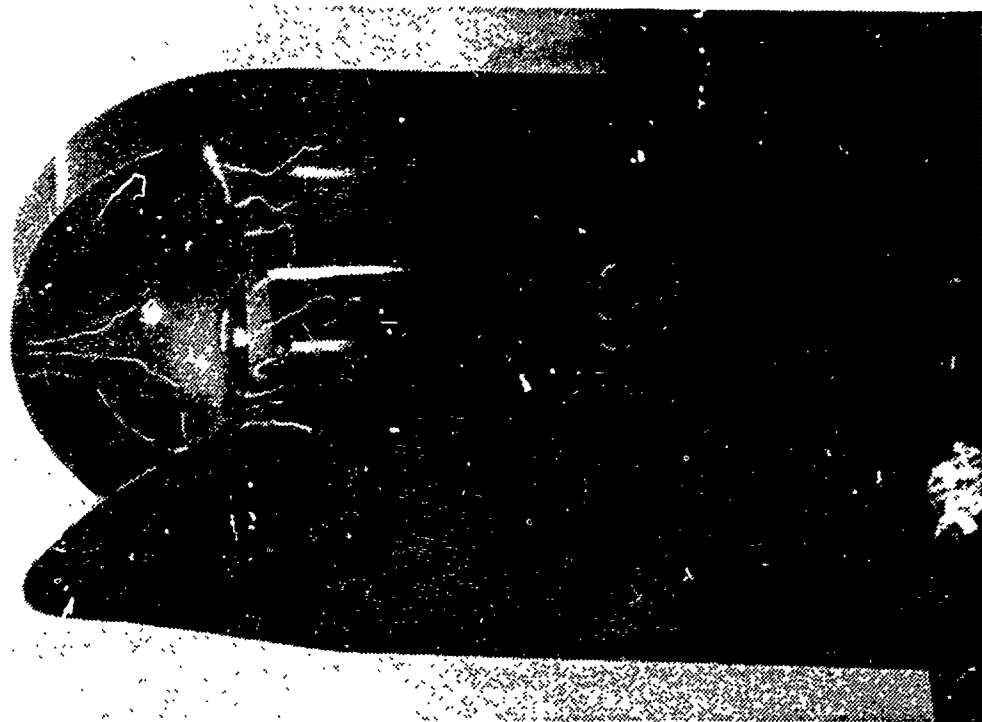


FIGURE IV-7. COMPLETE MODEL ASSEMBLY

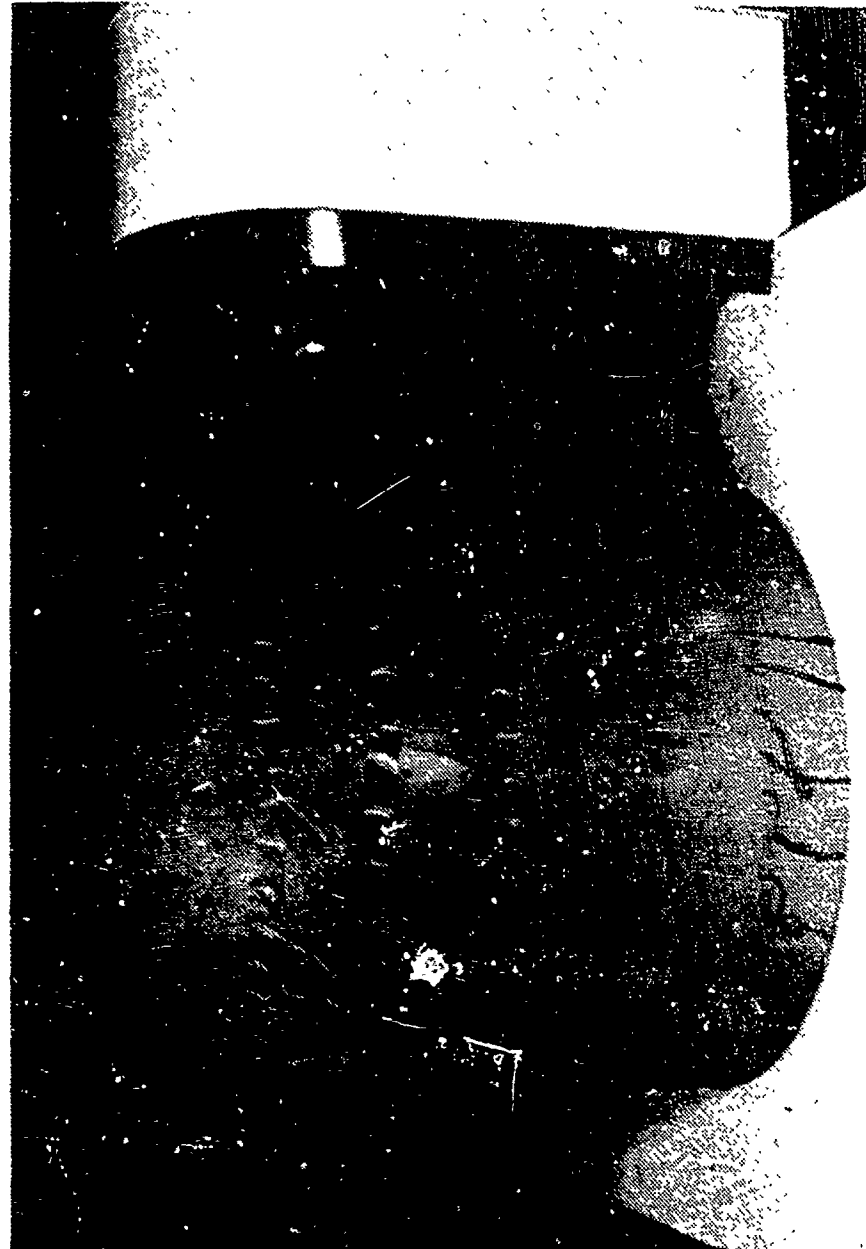


FIGURE IV-8. COMPLETE MCDEL ASSEMBLY



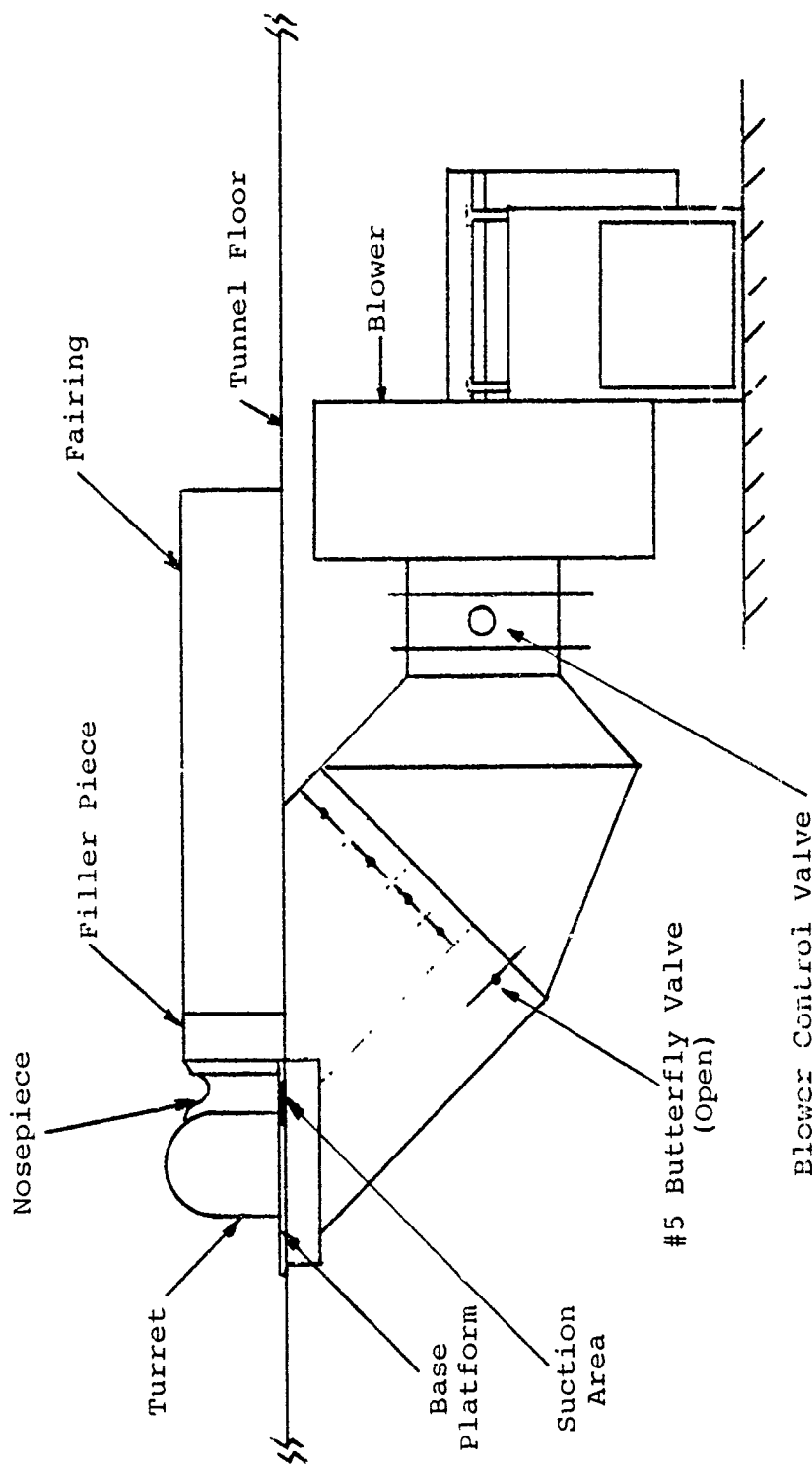


FIGURE IV-9. SIDE VIEW OF WIND TUNNEL MODEL AND BLOWER INSTALLATION

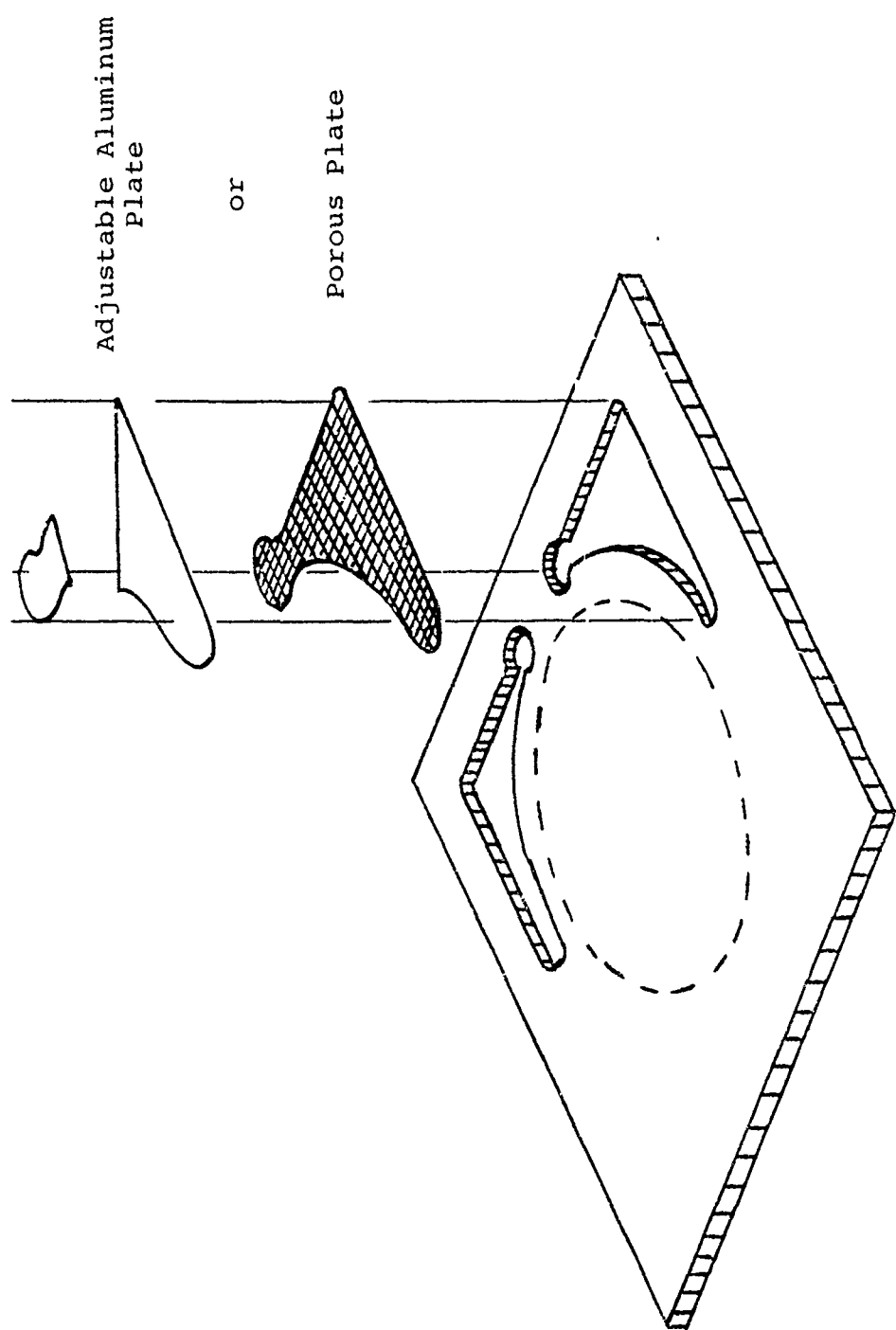


FIGURE IV-10. BASE PLATFORM WITH ADJUSTABLE HOLE CONTROLS

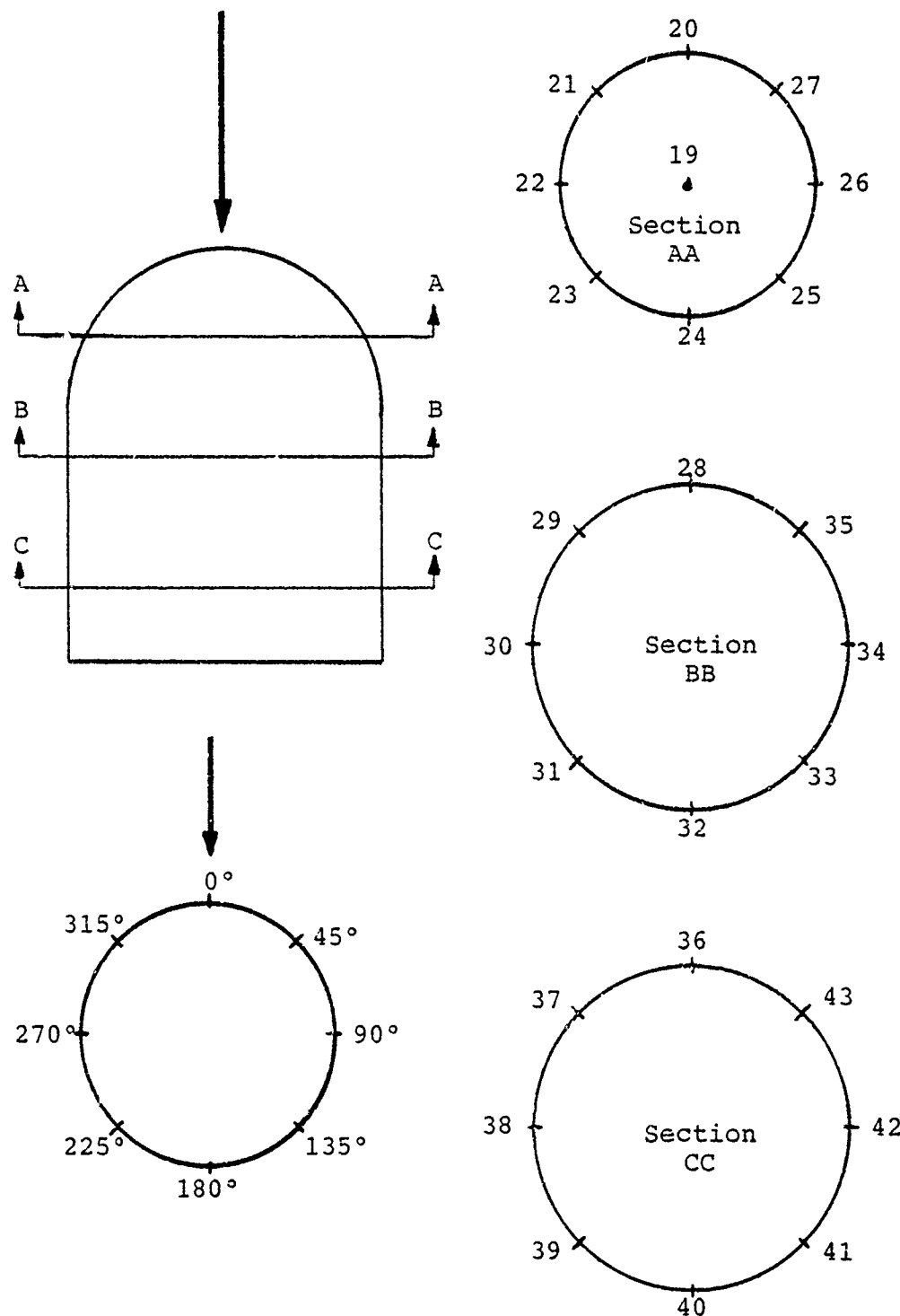


FIGURE V-1. TURRET PRESSURE TAP LOCATIONS

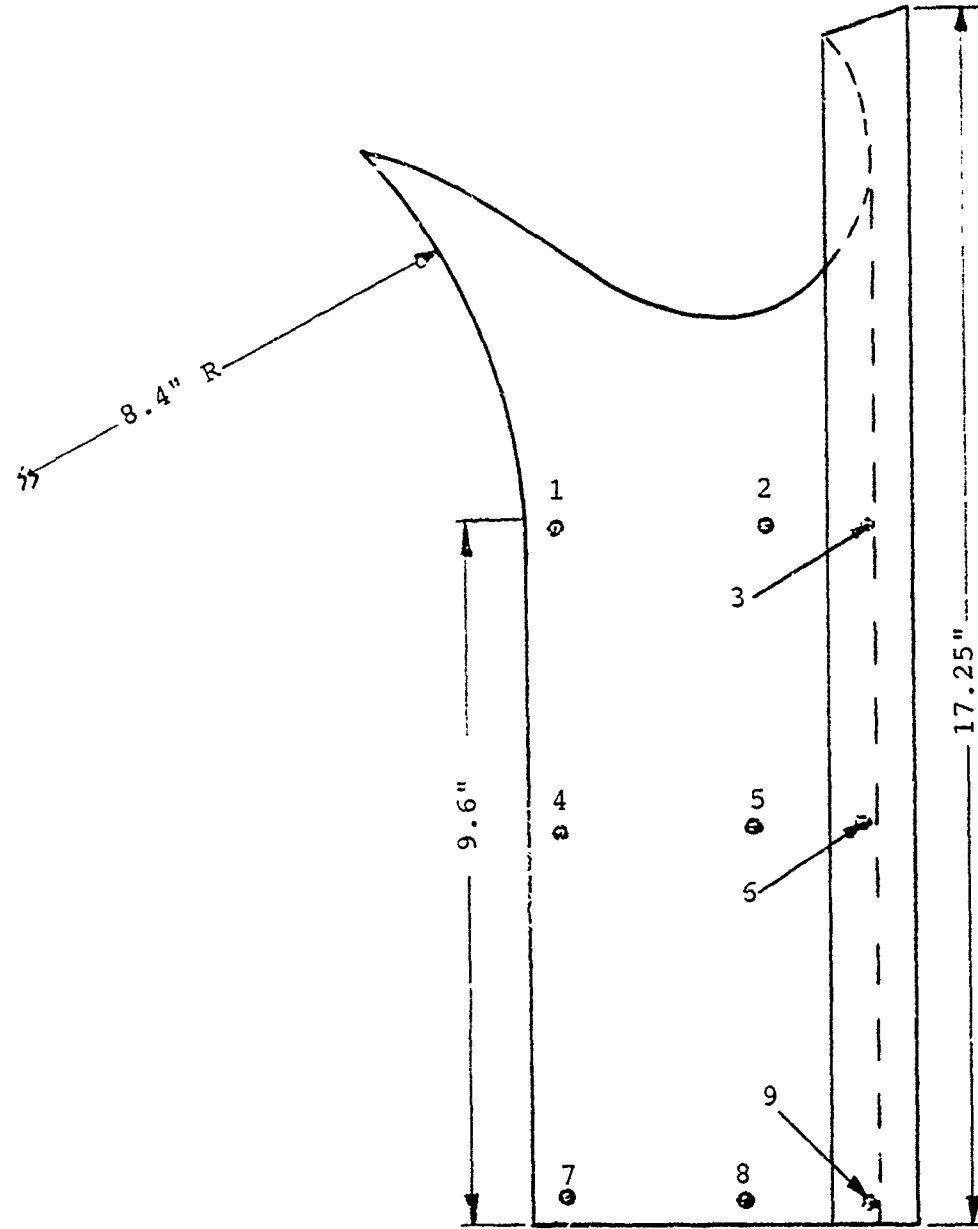


FIGURE V-2. NOSEPIECE PRESSURE TAP LOCATIONS

FIGURE V-3. DATA ACQUISITION SYSTEM



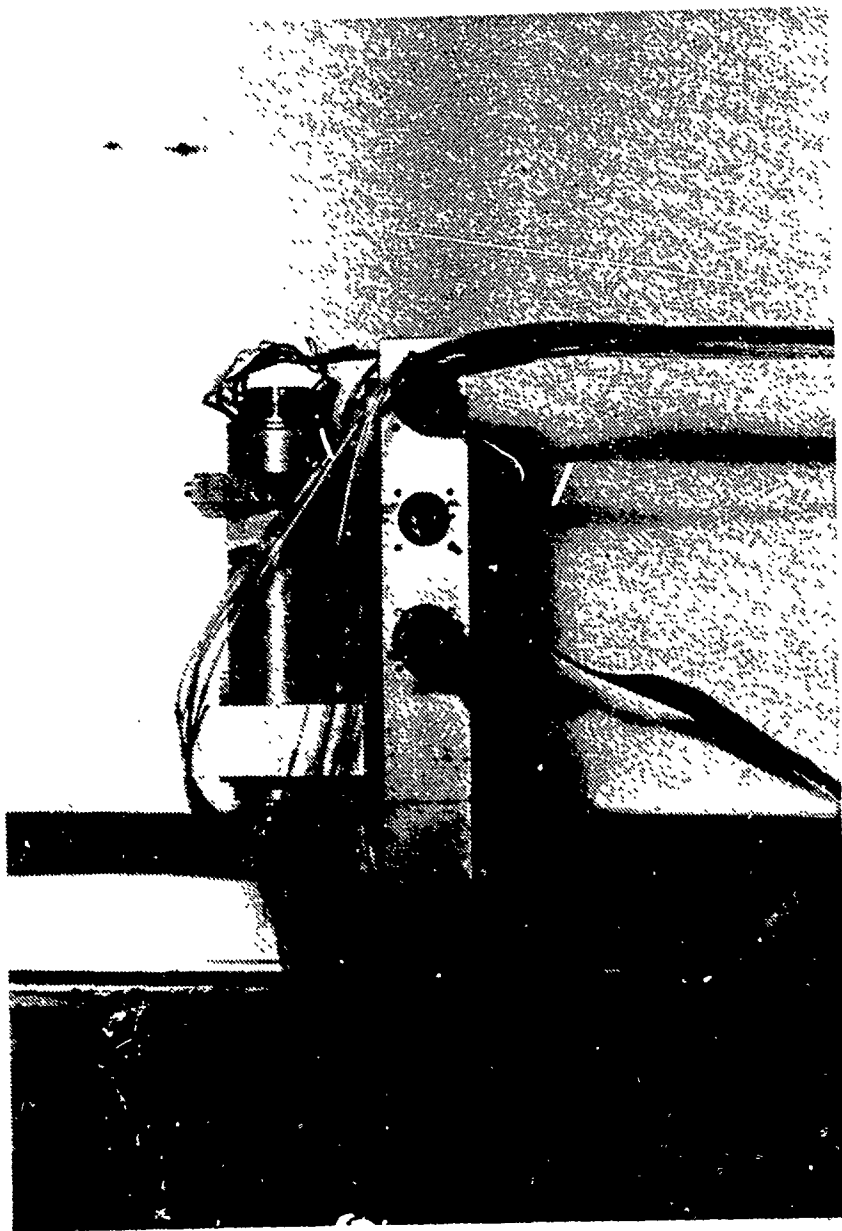


FIGURE V-4. SCANIVALVE

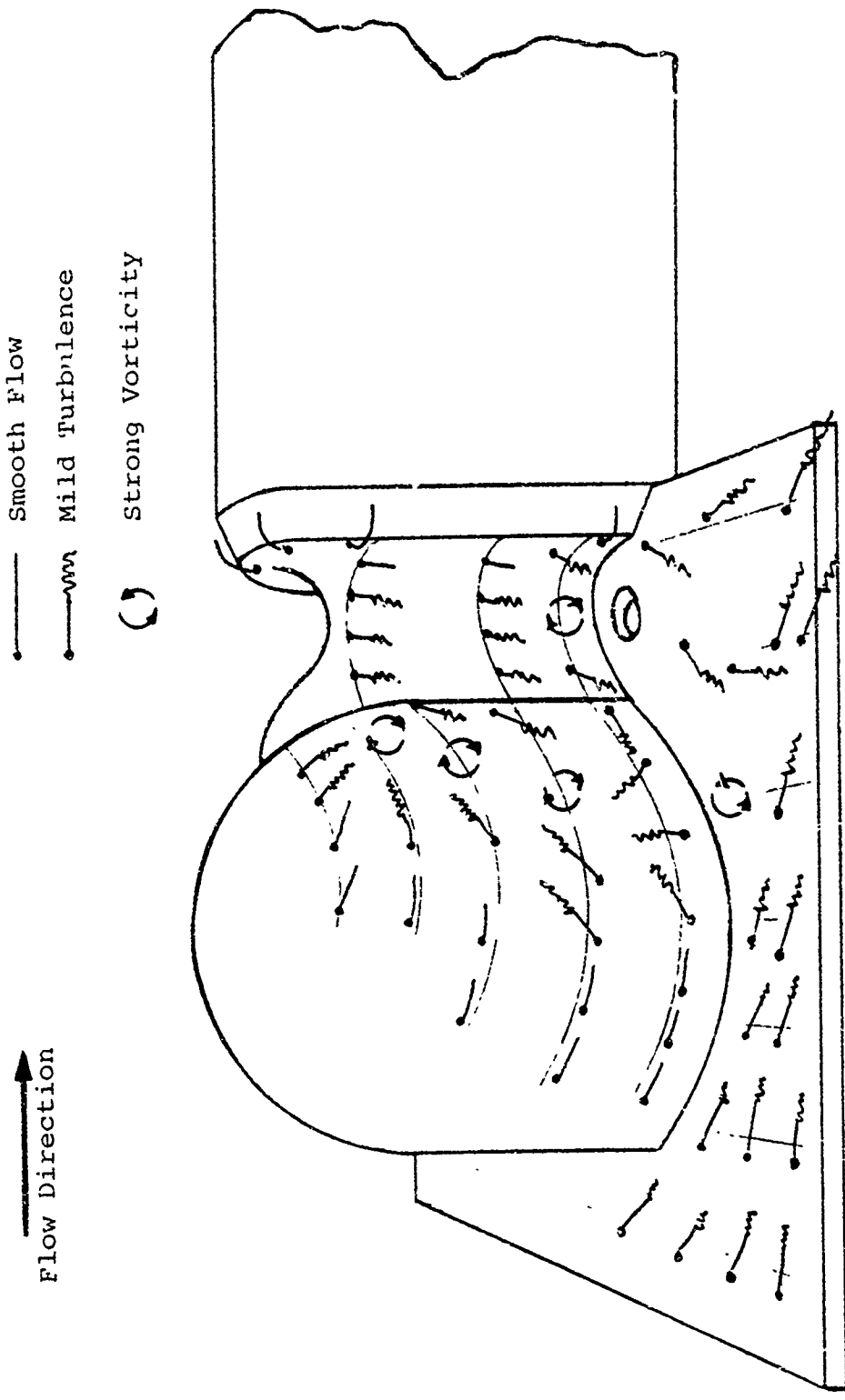


FIGURE VI-1. FLOW MAPPING, NO SUCTION

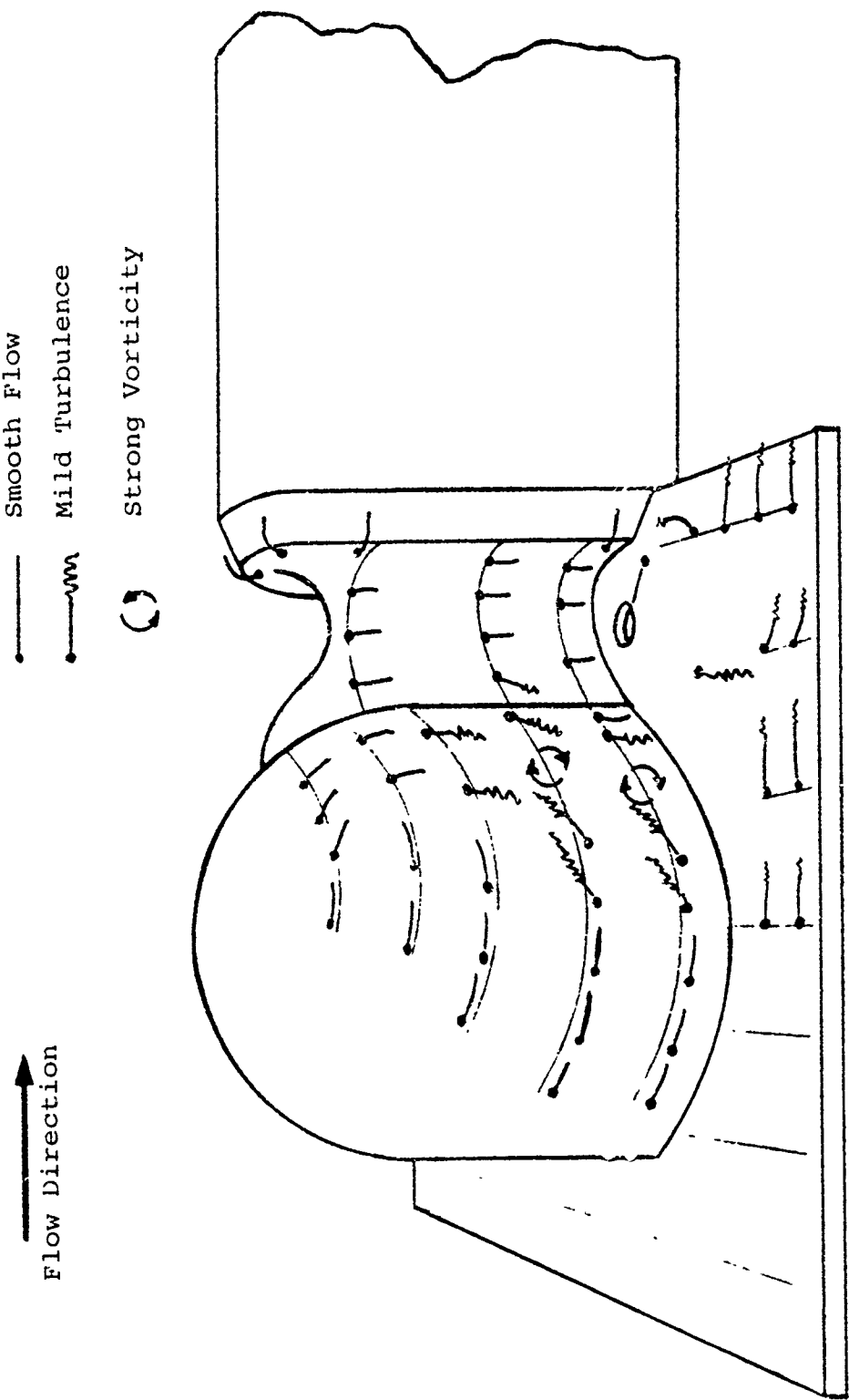


FIGURE VI-2. FLOW MAPPING, SUCTION THROUGH A 2.5 INCH DIAMETER HOLE

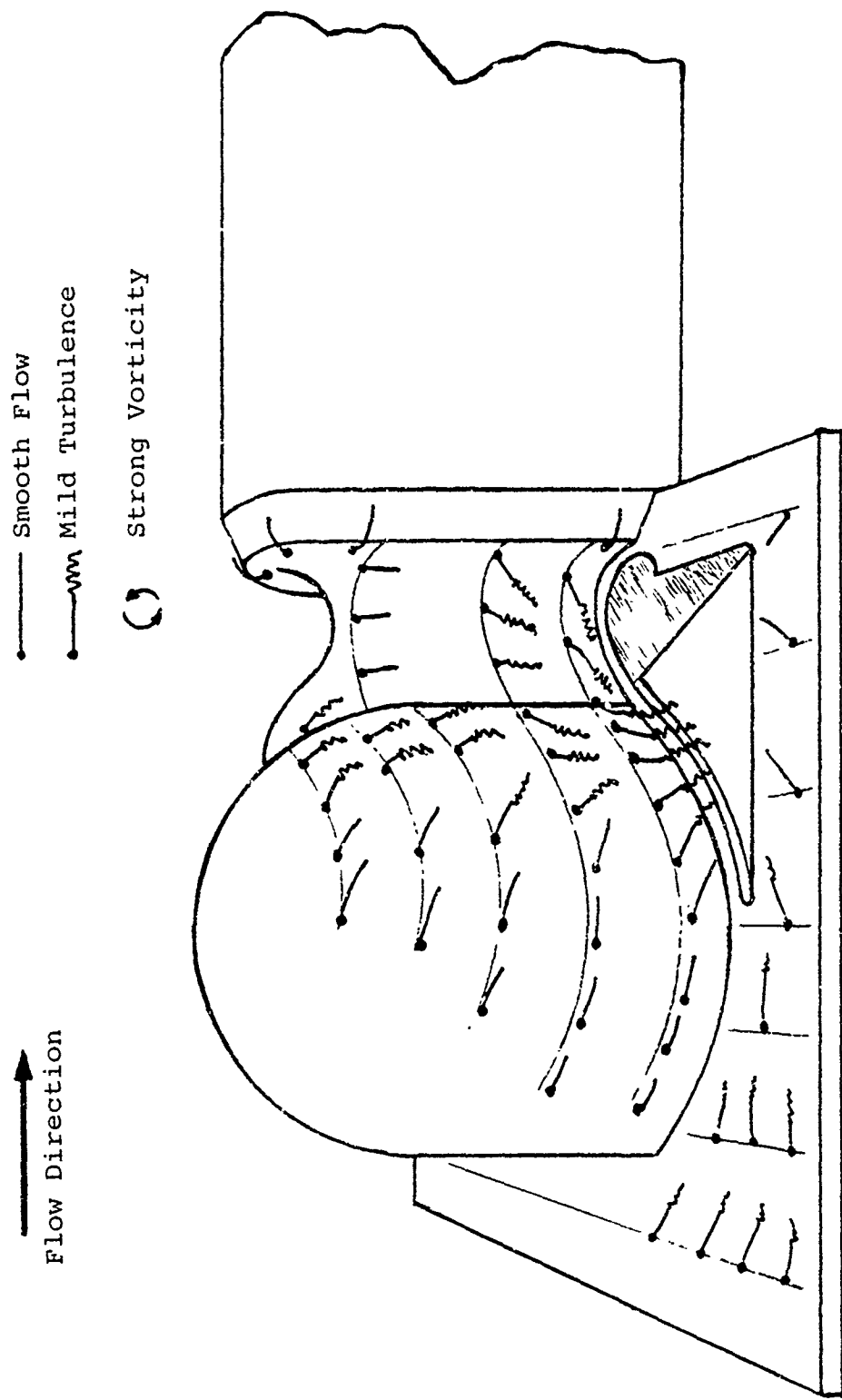


FIGURE VI-3. FLOW MAPPING, SUCTION WITH AFT AREA CLOSED

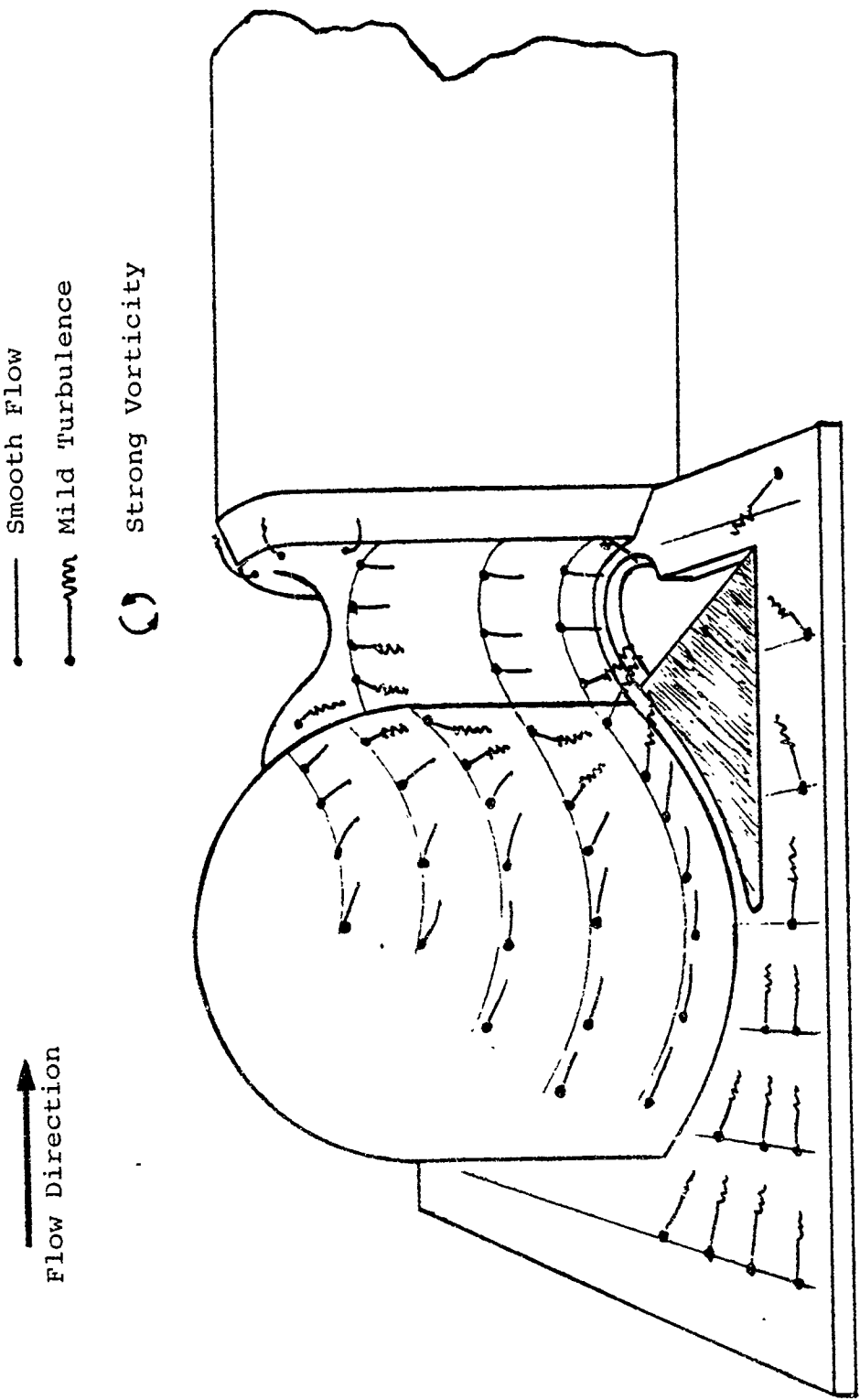


FIGURE VI-4. FLOW MAPPING, SUCTION WITH FORWARD AREA CLOSED

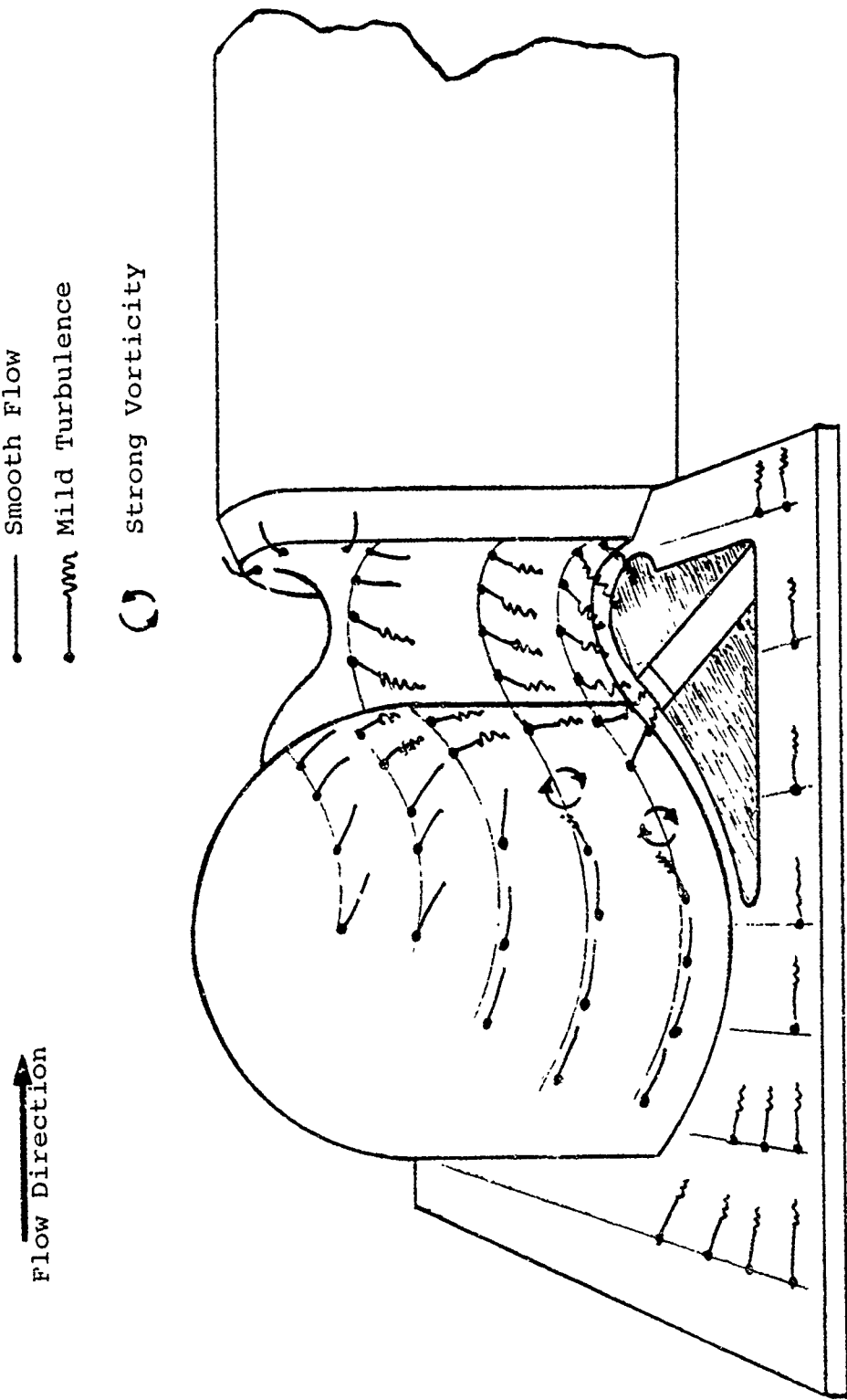


FIGURE VI-5. FLOW MAPPING, SUCTION THROUGH 2 INCH SLOT

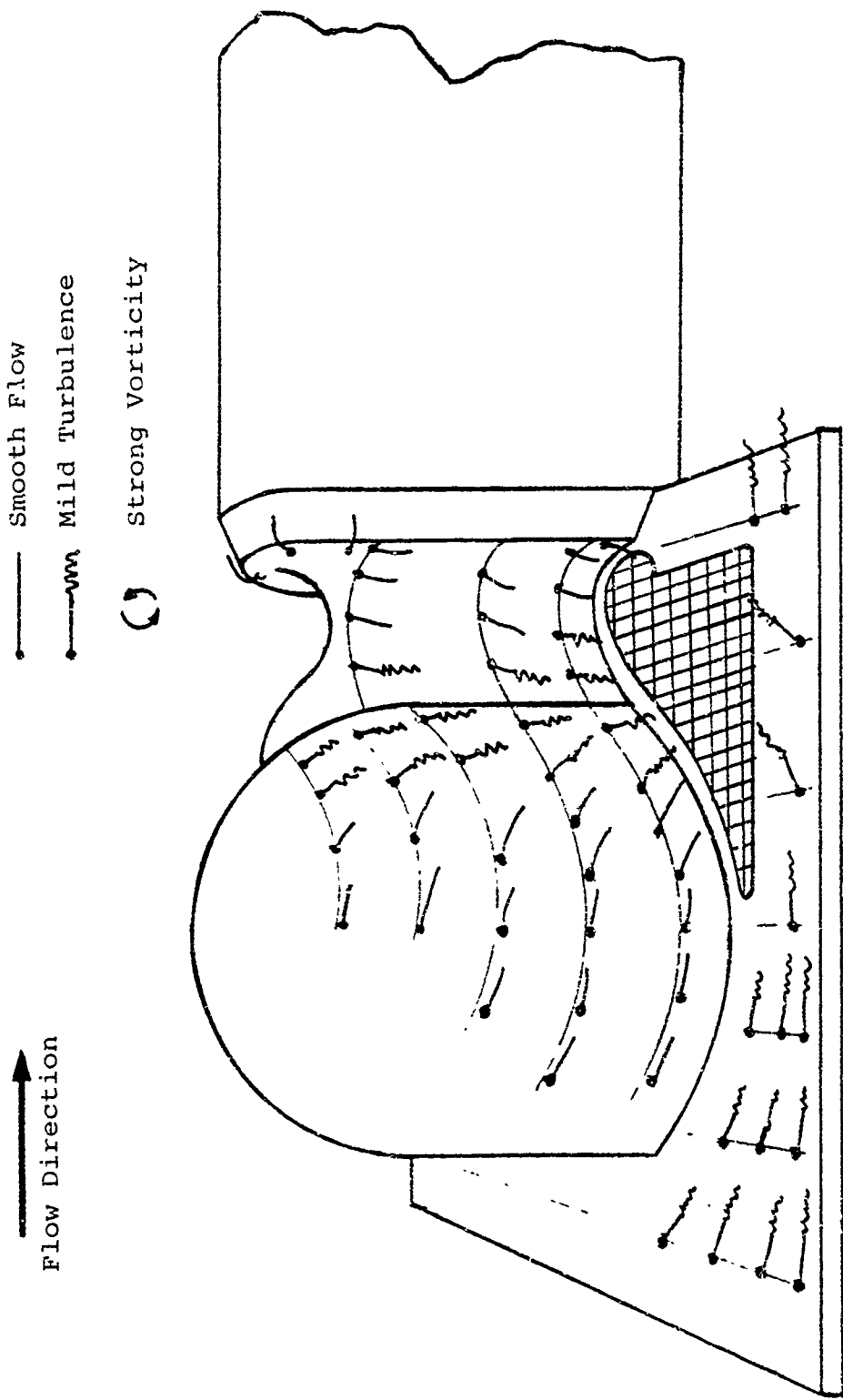
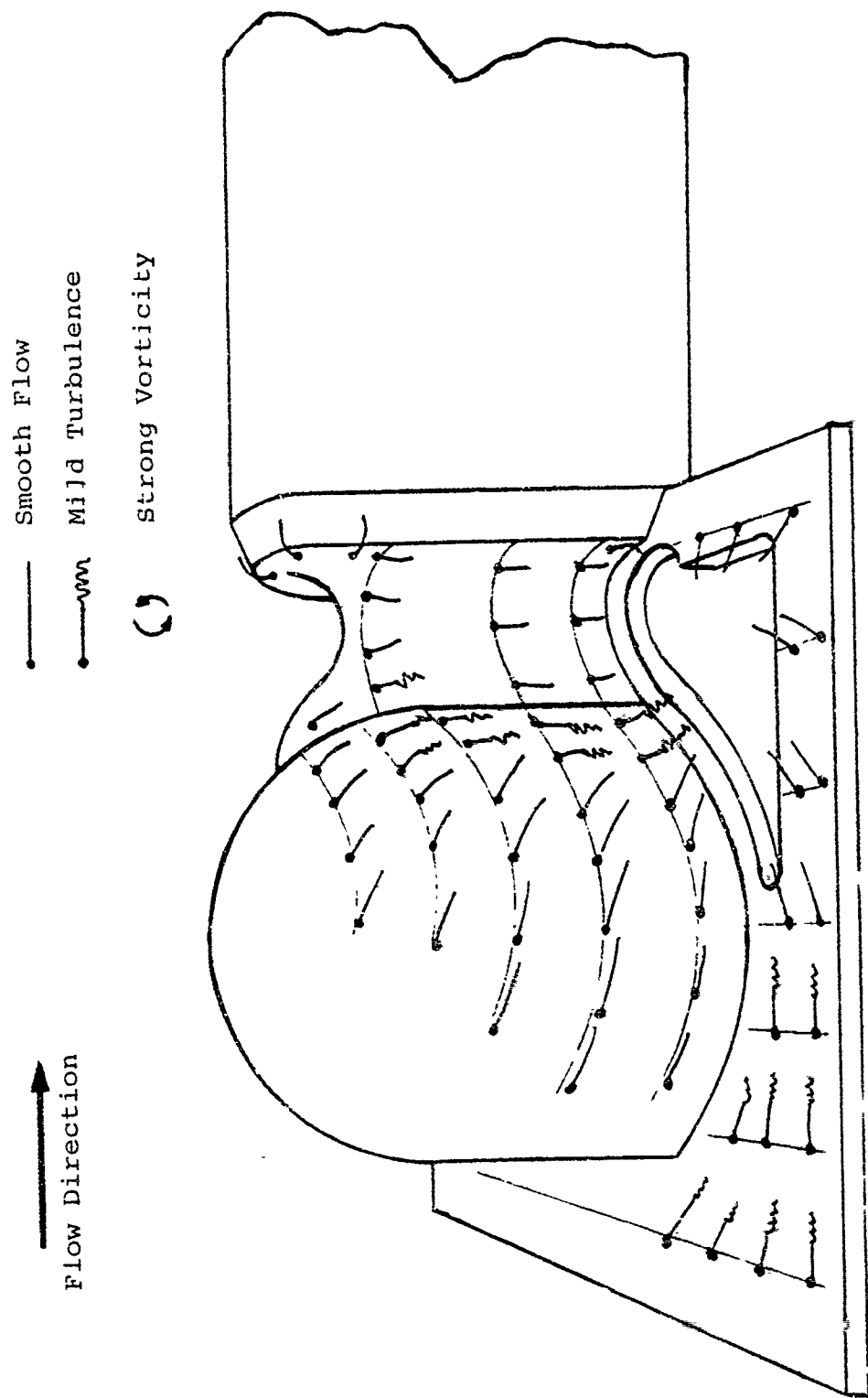


FIGURE VI-6. FLOW MAPPING, SUCTION THROUGH POROUS PLATE

FIGURE VI-7. FLOW MAPPING, SUCTION WITH LARGE HOLE OPEN



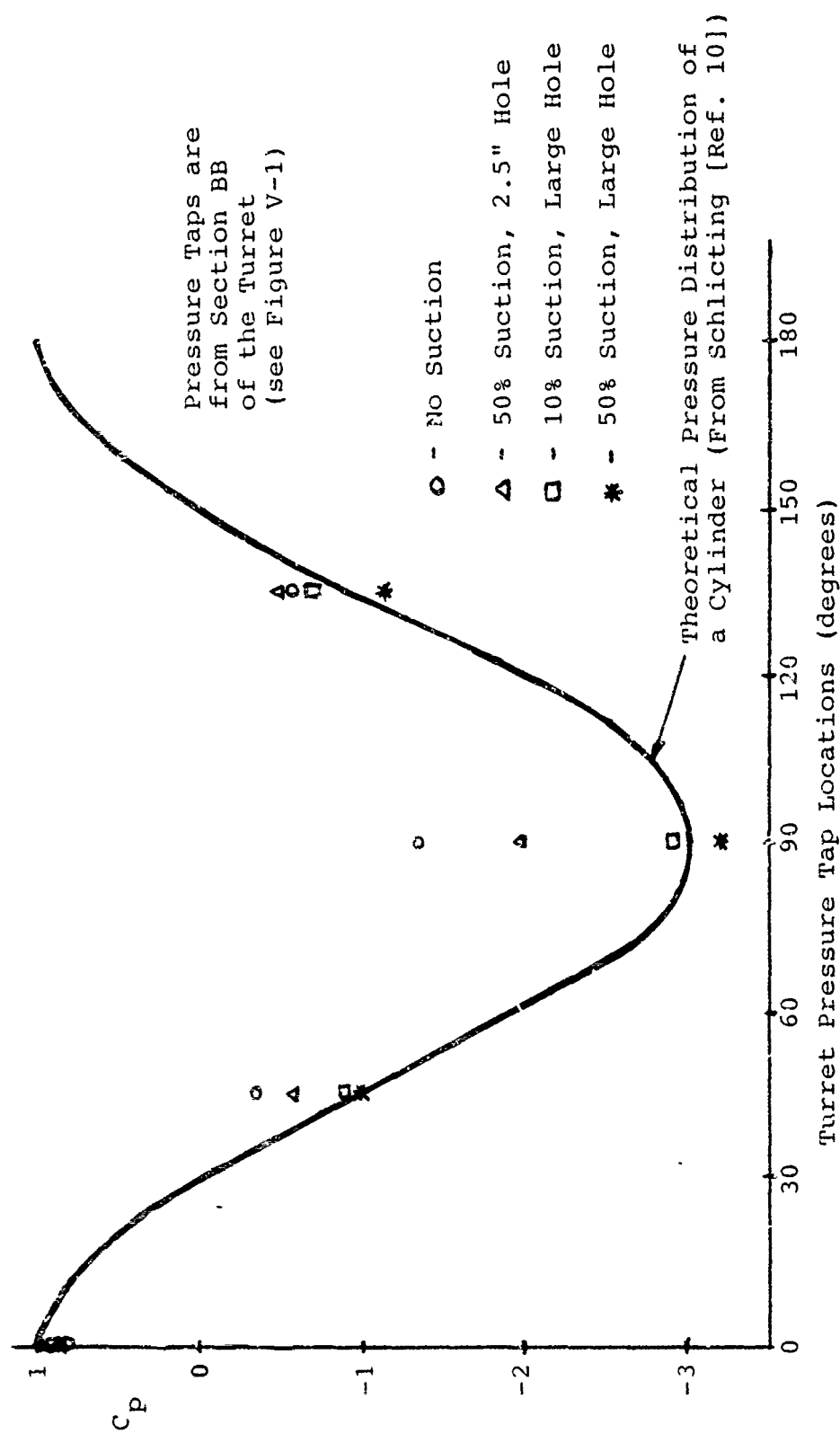


FIGURE VI-8. EXPERIMENTAL DATA PLOTTED WITH THEORETICAL PRESSURE DISTRIBUTION OF A CYLINDER

```

COMMON/VAL/X(50),Y(50),X1,Y1,THETA(50),B(50),E(50)
COMMON/DA/PI,I,X2,Y2,F,PAI
CCCOMMON/CA1/NN,II,ANGLE,ALPHA,R,PHI,C1,C2,PHIJ,PHIJ1
INTEGER N,I,J,K,M,N1
REAL NN,II,ANGLE,ALPHA,R,PHI,C1,C2,PHIJ,PHIJ1
REAL A(50,50),D(50,50)
REAL ERR,EE,STCRE,C(50),COLD(50),V(50),CP(50)
M=99
C ENTER THE NUMBER, N OF PANELS - MODIFY 200 FORMAT TO SUIT
N=30
N1=N+1
NN=FLOAT(N)
PI=ATAN(1.0)/45.0
PAI=PI*180.
PAIM=-PAI
READ(1,*) ALPHA,ERR,ICASE
C ALPHA SPECIFIES THE LOCATION OF START OF FIRST PANEL
C ERR SPECIFIES THE REQUIRED ACCURACY FOR ITERATION
READ(1,*) X2,Y2,F
DO 1 I=1,N1
  II=FLCAT(I)
C COORDINATES OF START OF PANEL I TO BE FED IN
  IF(ICASE.EQ.1)CALL DATA1
  IF(ICASE.EQ.2)CALL DATA2
1 CONTINUE
  DO 2 I=1,N
    IF(ICASE.EQ.1)CALL CASE1
    IF(ICASE.EQ.2)CALL CASE2
    WRITE(6,210) X(I),Y(I),THETA(I)
210 FORMAT(1H ,3(3X,F6.3))
  2 CONTINUE
  DO 3 I=1,N
    X1=(X(I)+X(I+1))/2.0
    Y1=(Y(I)+Y(I+1))/2.0
    DO 4 J=1,N
      R=((X1-X(J))**2+(Y1-Y(J))**2)/((X1-X(J))**2
      + (Y1-Y(J))**2)
      PHIJ=ATAN2(Y1-Y(J),X1-X(J))
      PHIJ1=ATAN2(Y1-Y(J+1),X1-X(J+1))
      C
      IF(Y(J).GT.Y1.AND.Y(J+1).LE.Y1)PHIJ=8.0*ATAN(1.0)+PHIJ
      PHI=PHIJ-PHIJ
      IF(PHI.GT.PAI)PHI=PHI-2.*PAI
      IF(PHI.LT.PAIM)PHI=PHI+2.*PAI
      ANGLE=THETA(J)-THETA(I)
      A(I,J)=-PHI*CCS(ANGLE)-0.5* ALOG(R)*SIN(ANGLE)
      IF(I.EQ.J) A(I,J)=4.0*ATAN(1.0)
      D(I,J)=PHI*SIN(ANGLE)-0.5* ALOG(R)*COS(ANGLE)
4 CONTINUE
3 CONTINUE
C ENSURE THE NUMBER AFTER THE , IS THE NUMBER OF PANELS
200 FORMAT(1H ,3(10F6.3//))
C WE NOW WISH TO SOLVE FOR THE PANEL SOURCE STRENGTHS C(I)
C MODIFY NEXT SECTION FOR A BETTER METHOD OF GETTING C(I)
  DO 10 I=1,N
    C(I)=C.0
10 CONTINUE
  DO 20 K=1,M
    EE=0.0
    DO 30 I=1,N
      COLD(I)=C(I)
      STCRE=B(I)
      DO 40 J=1,N
        IF(J.NE.I)STORE=STCRE-A(I,J)*C(J)
40 CONTINUE
      C(I)=STORE/A(I,I)
      EE=EE+ABS(C(I)-COLD(I))
30 CONTINUE

```

```

      IF(EE.LT.ERR)GC TC 50
20  CONTINUE
50  CONTINUE
      WRITE(6,220)K
220 FORMAT(1H,23HNUMBER OF ITERATIONS = ,I2)
      WRITE(6,250)
250 FORMAT(1H,29HTHE PANEL STRENGTHS, C(I) ARE)
      WRITE(6,200)(C(I),I=1,N)
C THIS CONCLUDES THE SOLUTION OF LINEAR EQUATIONS FOR C(I)
C NEXT OBTAIN THE VELOCITIES TANGENTIAL TO THE PANELS, V(I)
      DO 60 I=1,N
      V(I)=E(I)
      DO 70 J=1,N
      V(I)=V(I)+D(I,J)*C(J)
70  CONTINUE
C ALSO OBTAIN THE CORRESPONDING PRESSURE COEFFICIENTS CP(I)
      CP(I)=1.0-(V(I)**2)
60  CONTINUE
      WRITE(6,230)
230 FORMAT(1H,35HTHE TANGENTIAL VELOCITIES, V(I) ARE)
      WRITE(6,200)(V(I),I=1,N)
      WRITE(6,240)
240 FORMAT(1H,36HTHE PRESSURE COEFFICIENTS, CP(I) ARE)
      WRITE(6,200)(CP(I),I=1,N)
      WRITE(6,*)*X2,Y2,F
      STOP
END
SUBROUTINE DATA1
COMMON/VAL/X(50),Y(50),X1,Y1,THETA(50),B(50),E(50)
COMMON/DA/PI,I,X2,Y2,F,PAI
COMMON/DA1/NN,II,ANGLE,ALPHA,R,PHI,C1,C2,PHIJ,PHIJ1
REAL NN,II,ANGLE,ALPHA,R,PHI,C1,C2,PHIJ,PHIJ1
ANGLE=(180.0-ALPHA-360.0*(II-1.0)/NN)*PI
X(I)=COS(ANGLE)
Y(I)=SIN(ANGLE)
RETURN
END

SUBROUTINE CASE1
COMMON/VAL/X(50),Y(50),X1,Y1,THETA(50),B(50),E(50)
COMMON/DA/PI,I,X2,Y2,F,PAI
THETA(I)=ATAN2(Y(I+1)-Y(I),X(I+1)-X(I))
B(I)=SIN(THETA(I))
E(I)=COS(THETA(I))
RETURN
END

SUBROUTINE DATA2
COMMON/VAL/X(50),Y(50),X1,Y1,THETA(50),B(50),E(50)
COMMON/DA/PI,I,X2,Y2,F,PAI
READ(1,*) X(I),Y(I)
RETURN
END

SUBROUTINE CASE2
COMMON/VAL/X(50),Y(50),X1,Y1,THETA(50),B(50),E(50)
COMMON/DA/PI,I,X2,Y2,F,PAI
REAL NX,NY
X1=(X(I)+X(I+1))/2.
Y1=(Y(I)+Y(I+1))/2.
R12=(X1-X2)**2+(Y1-Y2)**2
R22=(X1-X2)**2+(Y1+Y2)**2
U=F/(2*PAI)*((Y1-Y2)/R12-(Y1+Y2)/R22)
V=-F/(2*PAI)*((X1-X2)/R12-(X1-X2)/R22)
THETA(I)=ATAN2(Y(I+1)-Y(I),X(I+1)-X(I))
NX=COS(THETA(I)-PAI/2.)
NY=SIN(THETA(I)-PAI/2.)

```

```

C     B(I)=SIN(THETA(I))
C     B(I)=U*NX+V*NY+SIN(THETA(I))
C     TX=COS(THETA(I))
C     TY=SIN(THETA(I))
C     E(I)=COS(THETA(I))
C     E(I)=U*TX+V*TY+CCS(THETA(I))
C     RETURN
C     END
C
C     INPUT DATA FOLLOWS
C
22.5,0.0001,2
2.4220,0.3200,0.6
0.0,0.0
0.1340,0.5
0.5,0.8660
1.0,1.0
1.5,0.8660
2.119,-0.2976
2.3000,0.1786
2.5500,0.1190
2.6500,0.1548
2.7300,0.2500
2.7500,0.3810
2.6800,0.6071
2.83,0.625
3.0700,0.625
8.5470,0.625
10.958,0.0
8.5470,-0.625
3.0700,-0.625
2.83,-0.625
2.6800,-0.6071
2.7500,-0.3810
2.7300,-0.2500
2.6500,-0.1548
2.5500,-0.1190
2.3000,-0.1786
2.119,-0.2976
1.5,-0.8660
1.0,-1.0
0.5,-0.8660
0.1340,-0.5
0.0,0.0

```

LIST OF REFERENCES

1. Rippel, David, Airborne Laser Turret Flow Control: A Parametric Study of Wind Tunnel Model Conditions, M.S. Thesis, Naval Postgraduate School, Monterey, California, 1981.
2. deJonckheere, Captain Richard, Control of Turbulent Separated Airflow about Aircraft Turrets, Workshop conducted at Air Force Weapons Laboratory, Kirtland Air Force Base, New Mexico, 10 and 11 March 1980.
3. Craig, James R., A Study in Flow Control and Screening Methods for Aircraft Laser Turrets, presented at workshop, Air Force Weapons Laboratory, Kirtland Air Force Base, New Mexico, 10 and 11 March 1980.
4. Prandtl, L., Über Flüssigkeitsbewegung bei sehr Kleiner Reibung (On Fluid Motions with Very Small Friction), Verhandlungen des III Internationalen Mathematiker Kongresses (Heidelberg, 1904), Leipzig, 1905.
5. Pao, Richard H. F., Fluid Mechanics, John Wiley & Sons, Inc., 1961.
6. von Kármán, Th., Über den Mechanismus des Widerstandes, den ein bewegter Körper in einer Flüssigkeit erfährt, Nachr. Ges. Wiss. Göttingen, 1911-1912; with H. Rubach, Physik. Z. Vol. 13, p. 49, 1912.
7. Roshko, A., On the Development of Turbulent Wakes from Vortex Streets, NACA Technical Report 1191, 1954.
8. Kaufmann, Walther, Fluid Mechanics, McGraw-Hill Book Company, Inc., 1963.
9. Lewellen, W. S., Theoretical Models of the Tornado Vortex, paper presented at the Symposium on Tornadoes, Assessment of Knowledge and Implications for Man, Texas Tech University, Lubbock, Texas, 22 through 24 June 1976.
10. Schlichting, Hermann, Boundary Layer Theory, 6th Edition, McGraw-Hill, 1968.

11. Mandigo, Alan, Control of Airflow about a High Energy Laser Turret, M.S. Thesis, Naval Postgraduate School, Monterey, California, 1980.
12. Schenberger, James, Flow Control about an Airborne Laser Turret, M.S. Thesis, Naval Postgraduate School, Monterey, California, 1980.

A silent 16 mm movie is available on loan to interested parties. The movie shows turret tuft motion with and without flow control employed for different nosepiece designs. Requests should be directed to Professor Allen E. Fuhs, Code 67Fu, Department of Aeronautics, United States Naval Post-graduate School, Monterey, California 93940. Telephone: Commerical, (408) 646-2948, or AUTOVON, 878-2948.

INITIAL DISTRIBUTION LIST

	<u>No. Copies</u>
1. Defense Technical Information Center Cameron Station Alexandria, Virginia 22314	2
2. Library, Code 0142 Naval Postgraduate School Monterey, California 93940	2
3. Department Chairman, Code 67 Department of Aeronautics Naval Postgraduate School Monterey, California 93940	1
4. Distinguished Professor Allen E. Fuhs Code 67Fu Department of Aeronautics Naval Postgraduate School Monterey, California 93940	2
5. Captain Richard deJonckheere, USAF AFWL, ARLB Kirtland Air Force Base New Mexico 87177	7
6. Dean W. M. Tolles, Code 012 Dean of Research Naval Postgraduate School Monterey, California 93940	1
7. LCDR David A. Rippel 1302 - 39th Street N.W. Canton, Ohio 44709	2
8. LT James E. Burd 3926 Corral Canyon Road Bonita, California 92002	2
9. Peter Bellamy-Knights Department of Mechanics of Fluids Simon Engineering University of Manchester Manchester M139PL United Kingdom	1

10. Ralph Haslund
M/S 8H-29
Boeing Aerospace Company
Post Office Box 3999
Seattle, Washington 98124

1